Chapter - 3

CATALYST CHARACTERIZATION

CATALYST CHARACTERIZATION

3.1 Introduction

Catalyst characterization is an integral part of catalytic research and development programme. Most practical catalysts are highly complex materials, and a basic problem is how to correlate catalyst behaviour with their physical and chemical characteristics/properties.

The characterization of a catalyst provides information on three distinct but related sorts. These are : Chemical composition and Chemical structure, texture and mechanical properties and catalytic activity.

Chemical composition and Chemical structure refer to the elemental composition, proportions of individual phases present, surface composition nature and properties of surface functional groups. The structure of a catalyst refers to its geometric structure and morphology. The characterization of a catalyst in terms of its activity is a quantitative measure of the ability of the catalyst to carry out a particular chemical transformation under specified condition.

The complete characterization of supported catalysts is extremely difficult due to the inhomogeneous nature of the catalysts themselves. Accordingly a wide range of analytical and spectroscopic techniques have been applied to the problem.

A typical characterization of a supported metal complex would involve the study of physico-chemical nature of the support, followed by a careful record of the conditions under which the supported catalyst had been prepared.

Micro analysis for many of the elements present and application of spectroscopic techniques to study the response of the supported catalysts to probe molecules such as CO, H_2 and NO, all the approaches put together help to arrive at the possible structure of the metal complex on the polymer.

Present chapter deals with the physico-chemical characterization of poylmer bound and unbound complexes such as, chemical composition, moisture content, apparent bulk density, surface area, swelling and crushing strength. Spectroscopic studies have been utilized to investigate the coordination structure of polymer-metal complexes, oxidation state of central metal atom and crystallinity of the supported complexes using techniques such as UV-VIS, IR, EPR, X-Ray, SEM and ESCA. Thermal stability of the support and supported complex has been studied using the DTA and TG analysis. Based on the spectroscopic and physico-chemical characteristics the schemes have been proposed for the probable structure of the metal complexes on polymer matrices.

3.2 Apparent bulk density, moisture content and crushing strength

Apparent bulk density (Abd), per cent moisture and crushing strength of all polymer bound catalysts are given in Table-3.1.

Moisture content of the catalysts decreases with an increase in per cent crosslinking of polymer supports. Since, the polymer (i.e. polystyrene-DVB) support is hydrophobic in nature (1), the hydrophilic nature of the supported catalysts may be due to hydrogen bonding between water and amino groups of the ligands and coordination of water molecules with metal atom.

Table-3.1

Moisture content, Bulk density and Crushing strength of polymer bound catalysts.

Catalyst	Moisture content (wt%)	Bulk density (gm/ml)	Crushing strength (kg)
3PRu(III)TMDA	2.51	0.41	0.15
10PRu(III)TMDA	1.68	0.48	0.20
30PRu(III)TMDA	0.97	0.62	0.32
2.5ZKRu(III)TMDA	2.67	0.59	0.10
20ZKRu(III)TMDA	1.09	0.75	0.24

Apparent bulk density was observed to be increased with an increase in the crosslinking of polymer. It is an important practical parameter because, it is indicative of the mass of catalyst packed into a reactor of specified volume. If the polymer supported catalyst is employed in a liquid phase slurry reactor, the Abd may not play any significant role, as the volume occupied by swollen polymer is more than the dry polymer and the swelling capacity differs with the solvents. In addition, it has a poor mechanical strength in the swollen state. However, it may be an useful parameter if the catalyst is introduced in the vapour phase reactor.

Crushing strength increases with an increase in per cent crosslinking. This is obvious and can be explained on the basis that increase in crosslinking the rigidity also increases.

3.3 Chemical composition

Elemental analysis of carbon, hydrogen, nitrogen, chloride and ruthenium for polymer bound ruthenium complexes of trimethylenediamine at various stages of reaction is given in Tables 3.2 - 3.3. The number of ligand molecules attached with the polymer were calculated by the difference of the two chloride ions (estimated gravimetrically) before and after introduction of the ligand. The calculated and experimental values were found to be in close agreement. Low loading of the metal and hence the chelation on the polymer matrix was achieved by carrying out the complexation reaction under mild conditions in presence of a good swelling agent.

In all the polymer anchored ruthenium complexes the ligand to metal ratio is high. This may be due to non accessibility of internal ligand molecules for the complex fomation (2).

Table-3.2

Elemental analysis and metal loading at different stages of reaction for poly(Sty-DVB) bound ruthenium catalysts.

Polymer cross-link	A			B			C			
	C (wt%)	H (wt%)	Cl (wt%)	C (wt%)	H (wt%)	N (wt%)	C (wt%)	H (wt%)	N (wt%)	Ru (wt%)x10^2
3	82.85	6.77	10.08	79.01	7.55	2.00	76.45	7.11	1.78	2.80
10	81.84	6.72	11.20	79.02	7.36	4.47	75.73	7.14	3.97	2.75
30	87.80	7.99	3.77	87.04	8.56	1.55	86.45	8.16	1.15	1.75

A = After chloromethylation B = after ligand insertion C = After complex formation

Table-3.3

Elemental analysis and metal loading at different stages of reaction for Zeo-Karb 226 bound ruthenium catalysts.

Polymer crosslink	A*		B*			C*			
	C (wt%)	H (wt%)	C (wt%)	H (wt%)	N (wt%)	C (wt%)	H (wt%)	N (wt%)	Ru (wt%)x10^2
2.5	53.48	7.50	53.92	8.63	2.84	53.32	8.22	2.42	3.4
20	64.94	7.49	65.49	5.22	5.42	65.12	7.98	5.24	0.56

* Estimation of oxygen is not carried out

A = Zeo-Karb 226 polymer B = after ligand insertion C = After complex formtion.

In general, polymer complex formation represents a complicated process. The polymer matrix swells after absorbing the solvents which changes the polymer structure. The swollen polymer then interacts with the metal ions and the complex formation takes place. It may be taken into account that each functional group (ligand) comes in contact with metal ions and coordinates with this to form "inner coordination complex". Then the special arrangement of the complexing groups over the polymer ligand chain takes various orientations with respect to the main chain. As a result, the total polymer complex as a whole is formed. The polymer complex formation also represents a relaxation process, which is related to the probability of transition of the system from one state of equilibrium to another.

3.4 **Surface area measurement**

Non-specific physical adsorption method (3,4) was used for the measurement of total surface area. Adsorption-desorption isotherms of nitrogen were recorded on a Carlo Erba Sorptomatic Series-1900 at -196°C (liquid nitrogen temperature) after degassing the sample at 75°C for 4 hours. From the adsorption-desorption isotherms, specific surface area and pore volume were calculated using BET equation.

The surface area and pore volume of the supports are given in Table-3.4. Surface area of all the supports were reduced to $\sim 1\ m^2g^{-1}$ after anchoring of the complexes. This could be due to blocking of pores of the support by the successive introduction of chloromethyl group, ligand and formation of metal complex.

Table-3.4

The surface area and pore volume of supports

Support	Surface area (M^2g^{-1})	Pore volume 10^2x(mlg^{-1})NTP
3P	7.78	1.64
10P	22.10	2.69
30P	55.14	3.11
2.5ZK	43.79	2.52
20ZK	65.44	4.74

3.5 Swelling studies

In order to achieve the higher activity and selectivity with polymer bound catalysts, it is necessary that the reactant molecules have accessiblity to all catalytic sites both on the surface and the interior of the beads. This requires the use of a solvent in which the polymer has a maximum swelling so that the matrix expands sufficiently to allow the reactant molecules to diffuse within the solvent channel and encounter the catalytic centers.

Extent of swelling depends on the polymer-solvent interaction which is determined not only by the nature of the solvent and the polymer matrix but also by the active groups attached to the polymer matrix.

In the present investigation an attempt has been made to ensure that the metal complexes are anchored uniformly during the synthesis and all catalytic centers are accessible during the reaction by studying the swelling of the support as well as the catalysts using ten different solvents of various nature (i.e. aliphatic, aromatic, polar and non-polar). The results are given in Tables 3.5-3.6 and shown in Figure-3.1.

It is found that the affinity of the polymer matrix for different solvents changes when functional groups and metal atoms are incorporated into it. Thus aliphatic non-polar n-heptane was found to be poor swelling agent, whereas dimethyl formamide, benzene, tetrahydrofuran, acetone and dioxane were noted to be good swelling agents. However, maximum swelling observed in water was probably due to the hydrogen bonding of water molecules with amino groups. In order to compare the catalytic activity of all the catalysts methanol (common solvent) was chosen as the medium.

Table-3.5

Swelling studies of Poly(Sty-DVB) bound ruthenium catalyst in different solvents.

Solvent	Swelling in mole %		
	3PRu(III)TMDA	10PRu(III)TMDA	30PRu(III)TMDA
Water	0.939	0.917	0.457
Methanol	0.639	0.619	0.198
Ethanol	0.289	0.272	0.099
Dioxane	0.162	0.139	0.081
N,N'dimethyl-formamide	0.152	0.125	0.080
Acetone	0.113	0.101	0.077
Tetrahydrofuran	0.111	0.090	0.076
Benzene	0.102	0.082	0.075
Cyclohexane	0.063	0.049	0.045
n-heptane	0.051	0.034	0.021

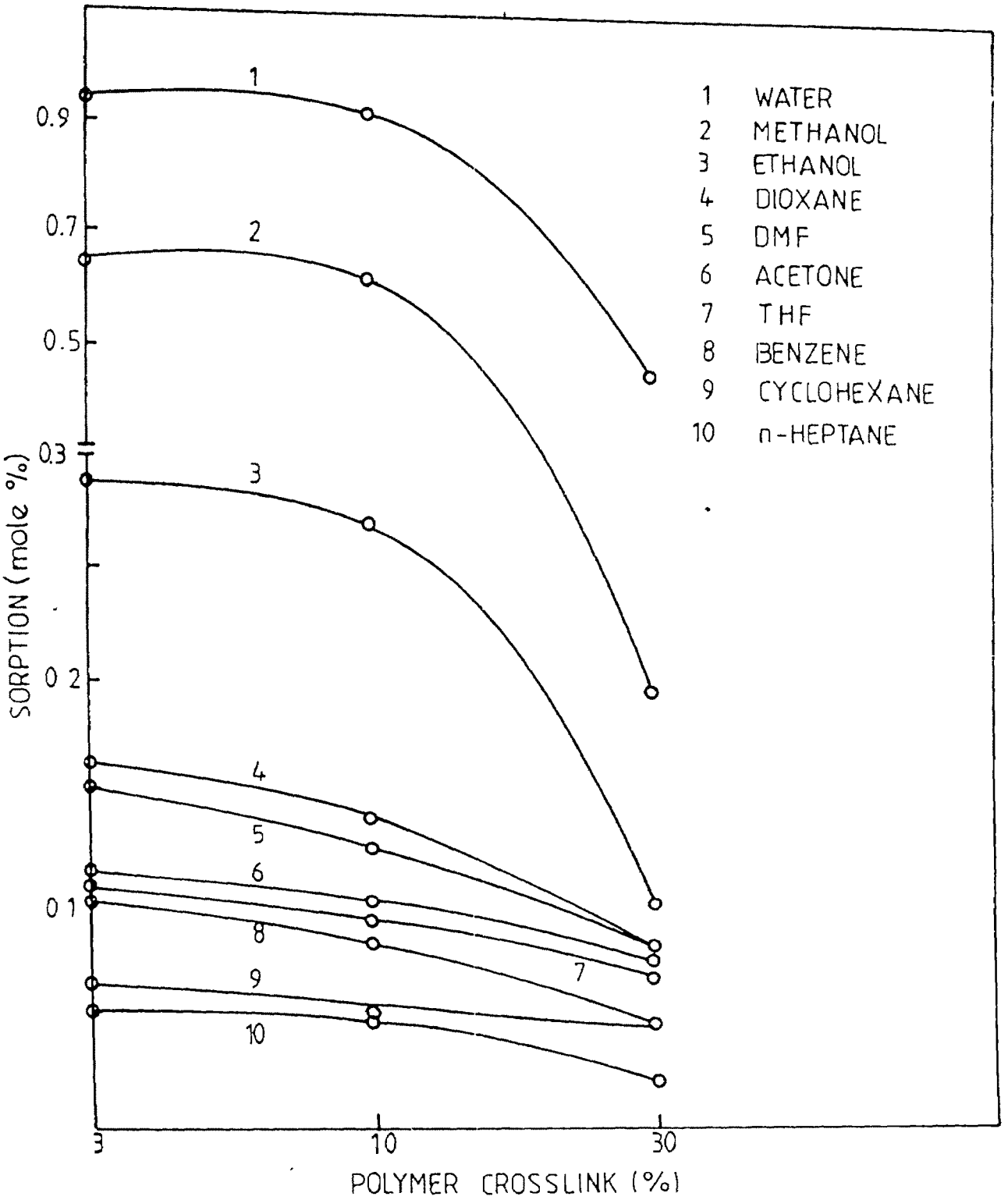

Figure-3.1 Swelling studies of poly(Sty-DVB) supported ruthenium catalysts.

Table-3.6

Swelling studies of Zeo-Karb bound ruthenium catalyst in different solvents.

Solvent	Swelling (mole %) 2.5ZKRu(III)TMDA	20ZKRu(III)TMDA
Water	4.43	1.09
Methanol	0.45	0.11
Ethanol	0.38	0.10
Acetone	0.27	0.09
N,N'dimethyl-formamide	0.25	0.08
Dioxane	0.24	0.07
Tetrahydrofuran	0.23	0.06
Benzene	0.21	0.05
Cyclohexane	0.14	0.04
n-heptane	0.09	0.03

3.6 Spectral characterization

3.6.1 UV-Visible spectroscopy (5-8)

The transitions involved in the UV-visible region (5000-50,000 cm^{-1}) are electronic. Thus d-d transitions are observable when degenerate d-orbitals are split by placing a transition metal ion in a crystal field. The splitting of the energy levels is affected by the number of d-electrons, the effective charge on the ion, the distribution and charge of the surrounding anions. Thus, information concerning the oxidation state and environmental symmetry of transition metal ions in catalysts are available. These transitions usually occur in the visible part of the spectrum. Charge transfer transitions involve more than one atom and include transitions from metal to ligand or vice versa, or between two neighbouring metal atoms of different oxidation state. Usually such trasitions occur in the UV region and do not mask the d-d transitions in the visible region. The technique employed in UV-visible spectroscopy for powdered samples involves the measurement of diffusely reflected light(6). However, a major difficulty exists in relating the measured diffused reflected light to the sample absorption in the presence of substantial scattering by sample.

Figures 3.2 and 3.3 show the UV-visible diffuse reflectance spectra recorded for polymer bound ruthenium catalysts, using $BaSO_4$ as standard.

In the case of polymer bound ruthenium complexes the broad absorption band including three peaks between 210 and 340 nm was assigned to d-d transitions of Ru(III), which was further confirmed by ESCA measurement.

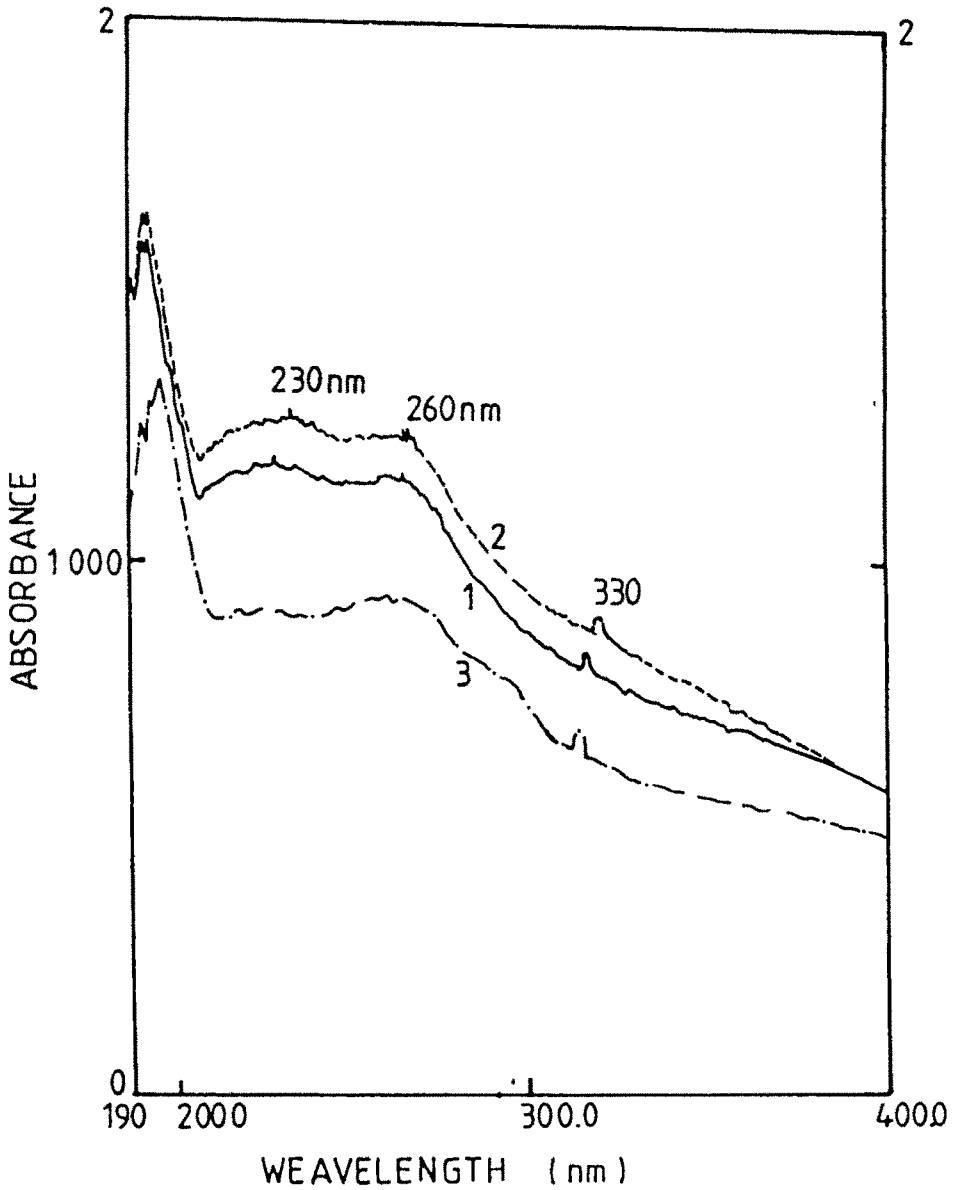

Figure-3.2 UV-Vis reflectance spectra of

1) 3PRu(III)TMDA 2) 10PRu(III)TMDA

3) 30PRu(III)TMDA

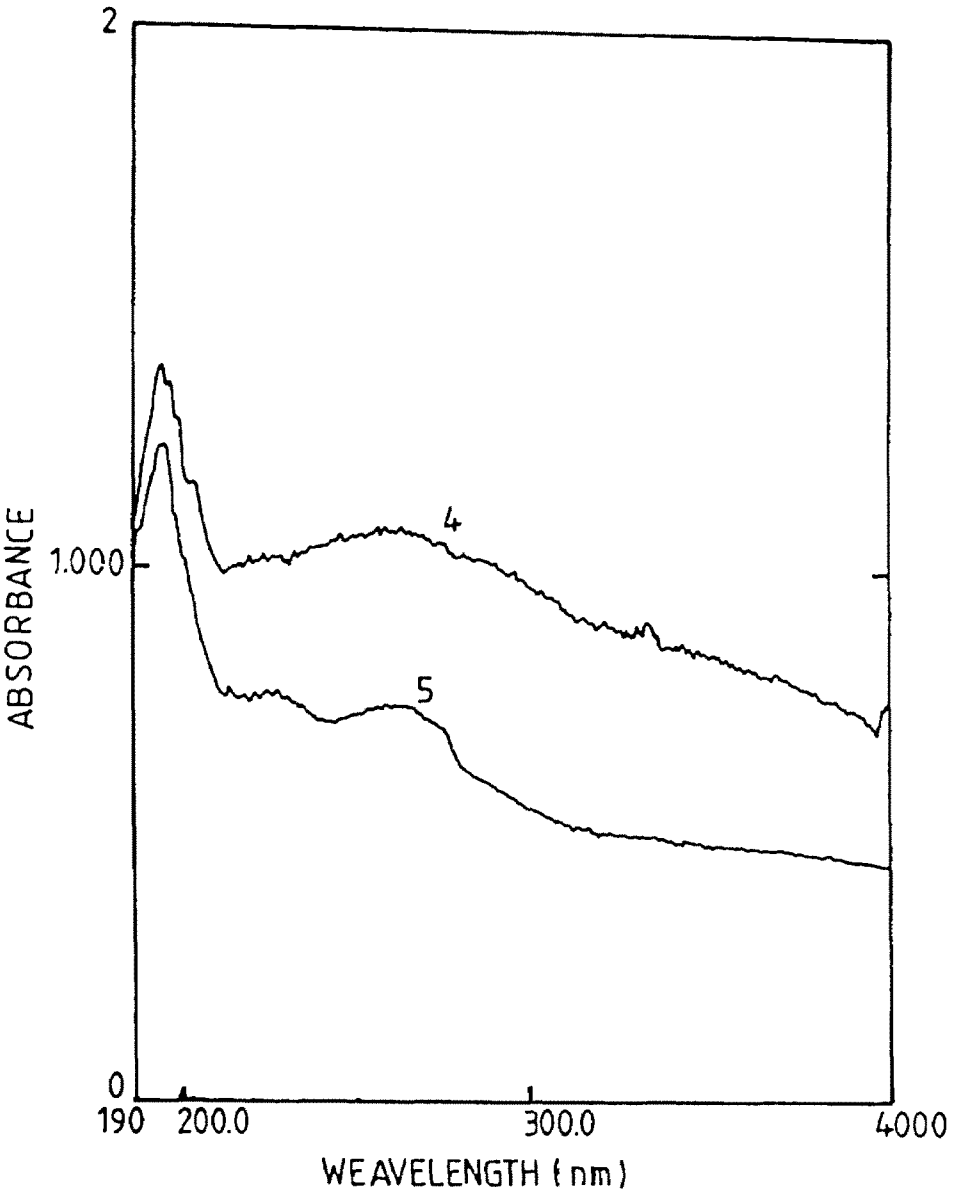

Figure-3.3 UV-Vis reflectance spectra of

4) 2.5 ZKRu(III)TMDA 5) 20ZKRu(III)TMDA

Figure-3.4 shows the UV-visible spectrum of unbound [RuTMDACl$_2$]Cl in methanol (13).

3.6.2 Infrared spectroscopy

Infrared spectroscopy has been widely used for the characterization of organometallic compounds. It provides a reliable information about the organic compounds in the IR (i.e. 600-4000 cm^{-1}) and that of metal-ligand vibrations in Far-IR (50-600 cm^{-1}) region. The formation of metal complex, the bond formed between the metal and coordinating atom of the ligand molecule can be understood by the nature and the position of the absorption bands.

Absorption spectra of polymer bound ligands or metal ions are changed some times drastically by complex formation. Since in a polymer bound metal complex, a huge macromolecular chain is adjacent to the coordinating groups, not only the kind of coordinating groups but also the environment around the metal complex are strongly influenced by the polymer chain. The IR absorption characteristics of a polymer bound metal complex in a solution as well as in a solid-state are dependent on such a micro-environment given by the polymer chain.

Since the absorption spectra of polymer bound complexes are highly complicated, interpretation of just a polymer bound catalyst will always be misleading. However, a detailed and comparative study of the absorption spectra of polymer support, functionalized support, after metal attachment and that of unbound complex will provide a fairly conclusive information.

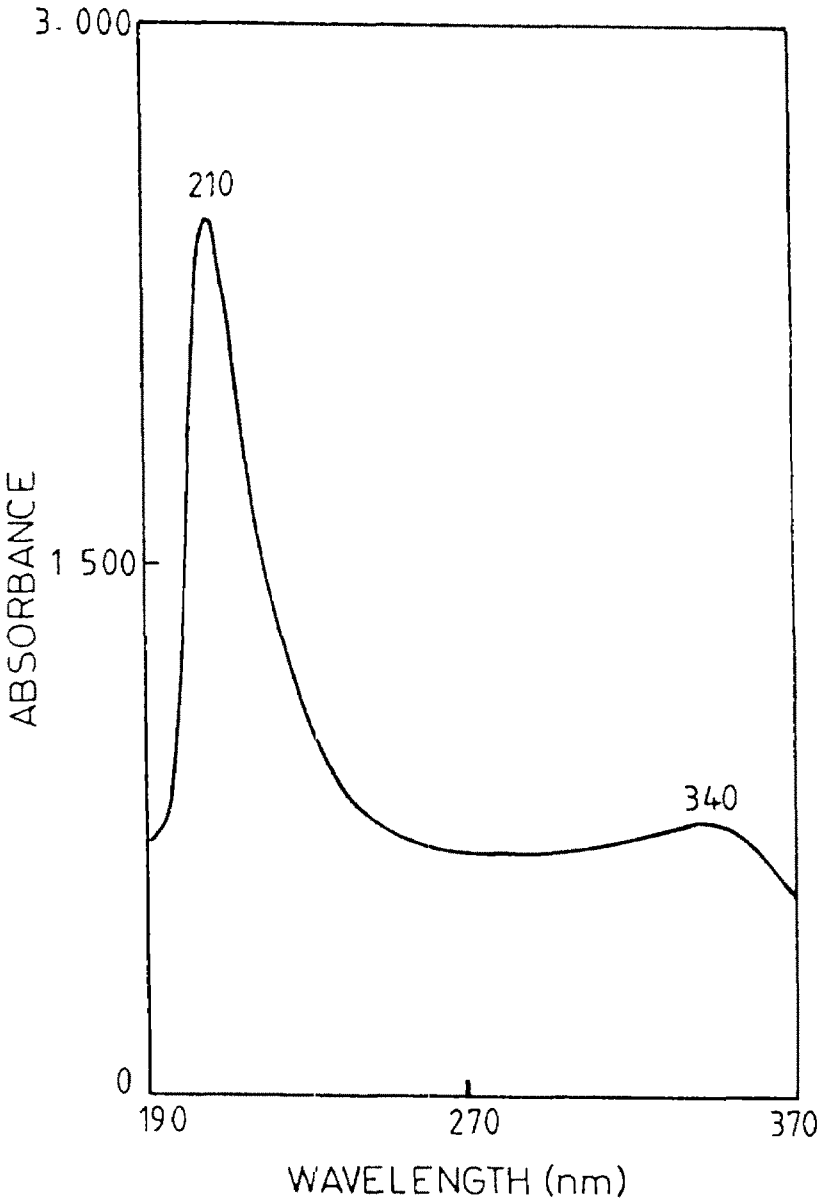

Figure-3.4 UV-Vis absorbance spectrum of $[RuTMDACl_2]Cl$ in methanol.

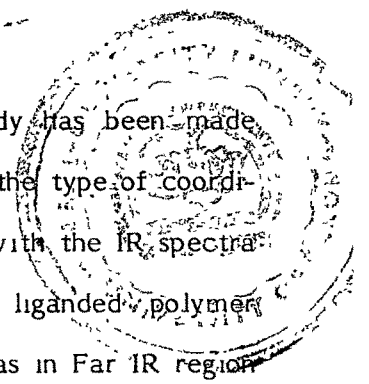

In the present investigation a detailed infrared study has been made to understand the mode of attachment of the ligands and the type of coordination with the metal ions by comparing them separately with the IR spectra of crosslinked polystyrene, chloromethylated polymer, liganded polymer and also corresponding unbound complex in the IR as well as in Far IR region are shown in Figures 3.5 to 3.12 respectively. From the Figure-3.5(b) an IR-band was found at 1235 cm^{-1} for $-CH_2Cl$ group. The IR absorption frequency of a ligand is usually shifted by complex formation with metal atom (9-10). A summary of the IR frequency assignment for polymer bound and unbound complexes (11-14) are given in Table-3.7.

An interesting observation about the mode of coordination of TMDA may be inferred from the IR spectral data. For these bidentate metal complexes, it is possible to identify the coordinated amino stretching frequencies. In the bidentate complex, containing TMDA, the free amino stretching frequency in the region 3500-3400 cm^{-1} could not be detected. This indicates that the amino group of TMDA is involved in the complex formation. Similar pattern of IR absorption is observed in the present study in the case of all polymer bound ruthenium catalysts for the amino groups (Figure-3.7-3.11).

However, it is clear from the micro analysis and metal loading, that all the attached ligand molecules are not involved in the complex formation. Even then, the formation of metal chelates could be concluded from the decrease in the intensities of amino absorption bands in the region 3400-3500 cm^{-1}, also from the appearance of new bands (due to chelation) Figures (3.7-3.11). Spectra of polymer bound catalysts were consistent with the IR spectrum of well characterized isolated similar unbound complex (Figure -3.12).

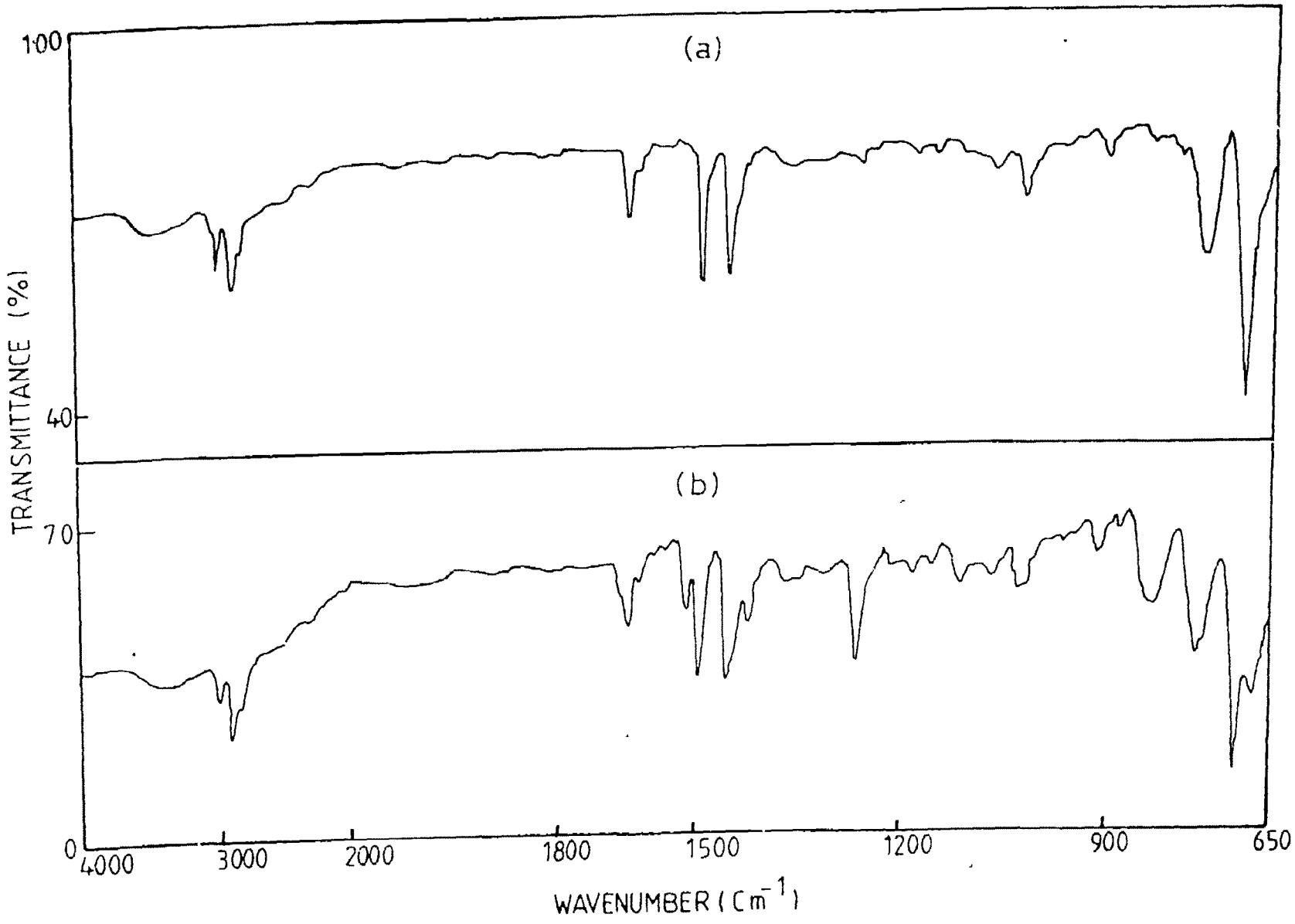

Figure-3.5 Infrared spectra of a) 3% crosslinked poly(Sty-DVB) b) Chloromethylated 3P

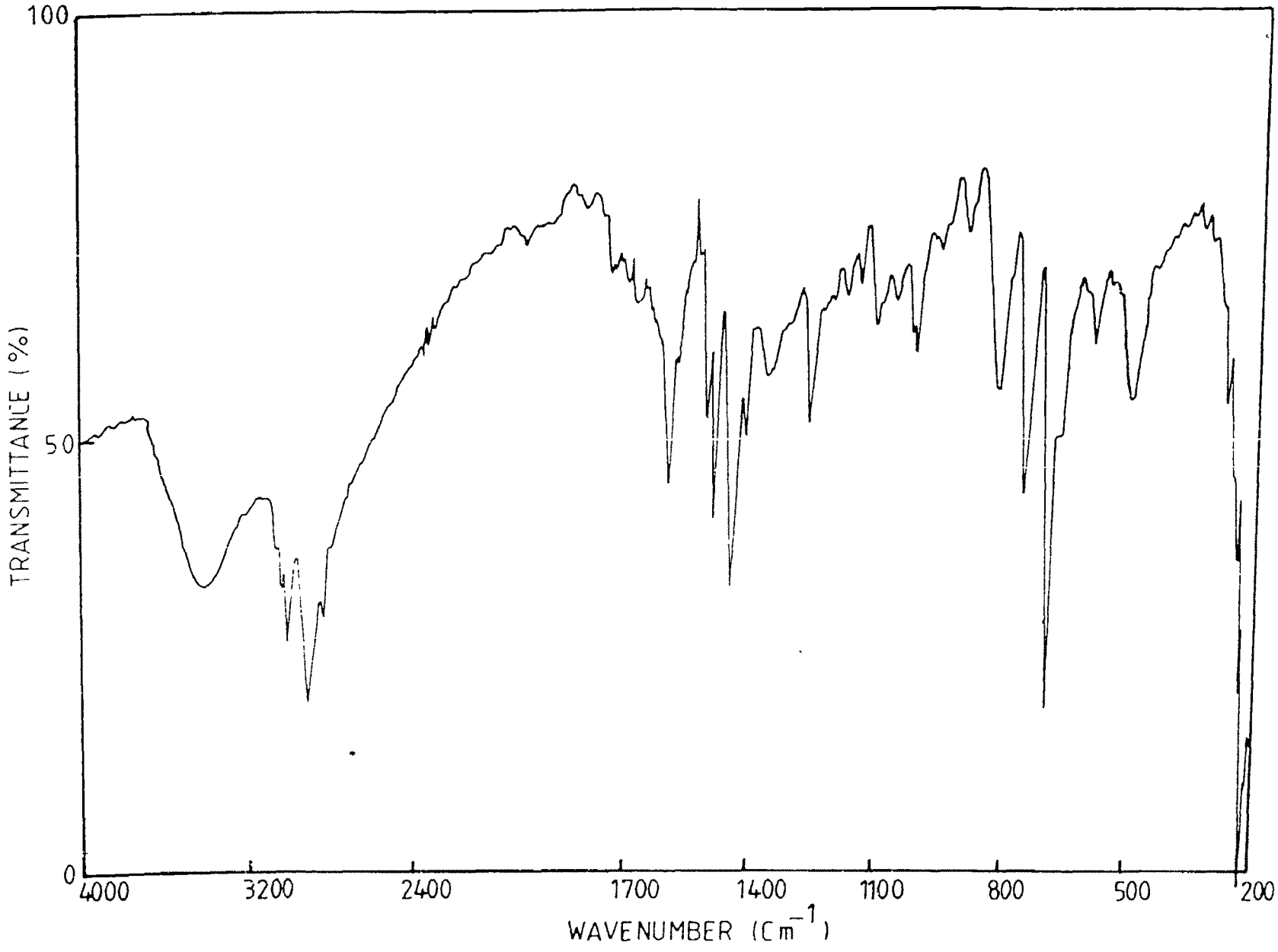

Figure-3.6 Infrared spectrum of liganded polymer i.e. 3PTMDA

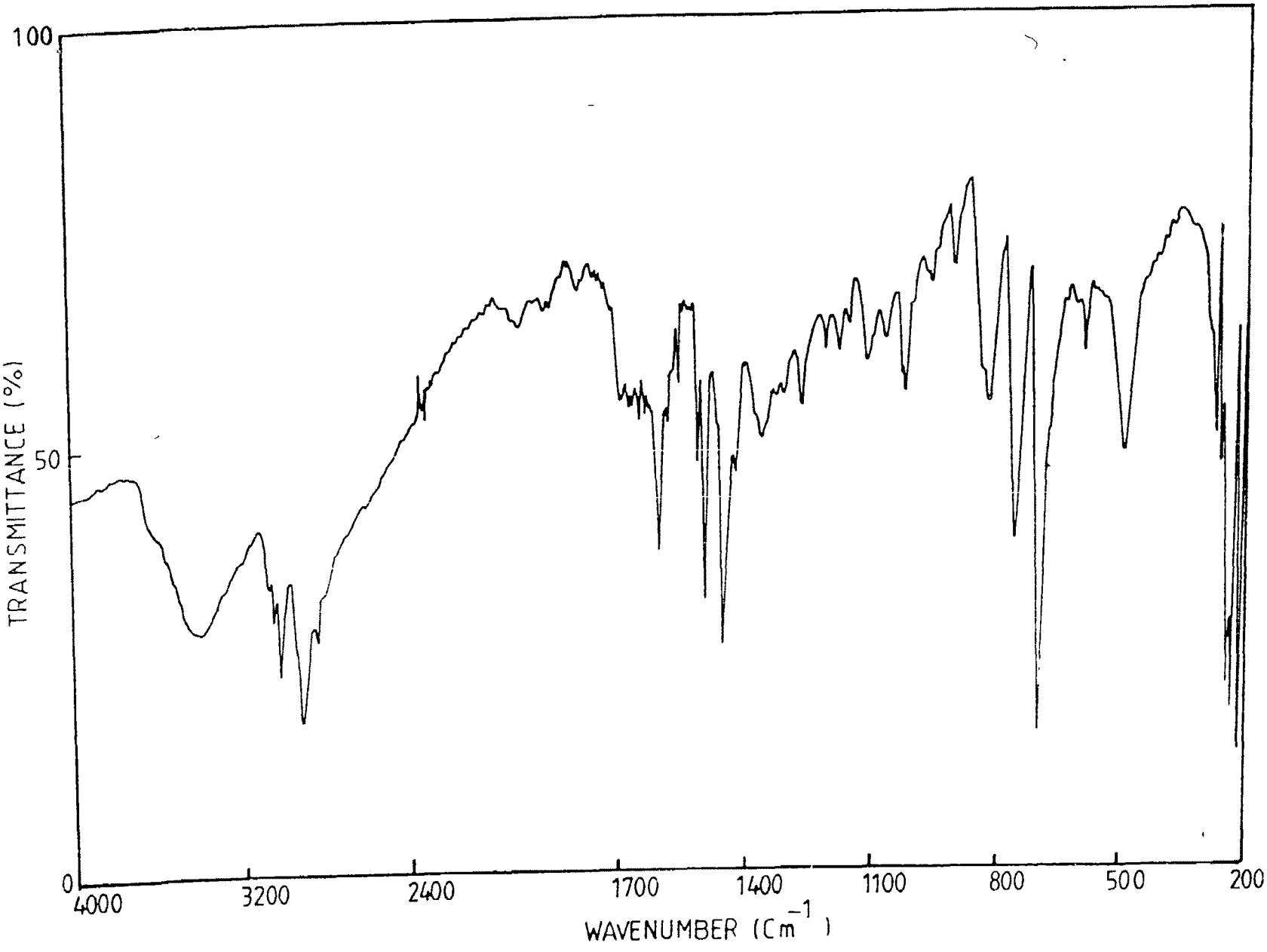

Figure-3.7 Infrared spectrum of 3PRu(III)TMDA

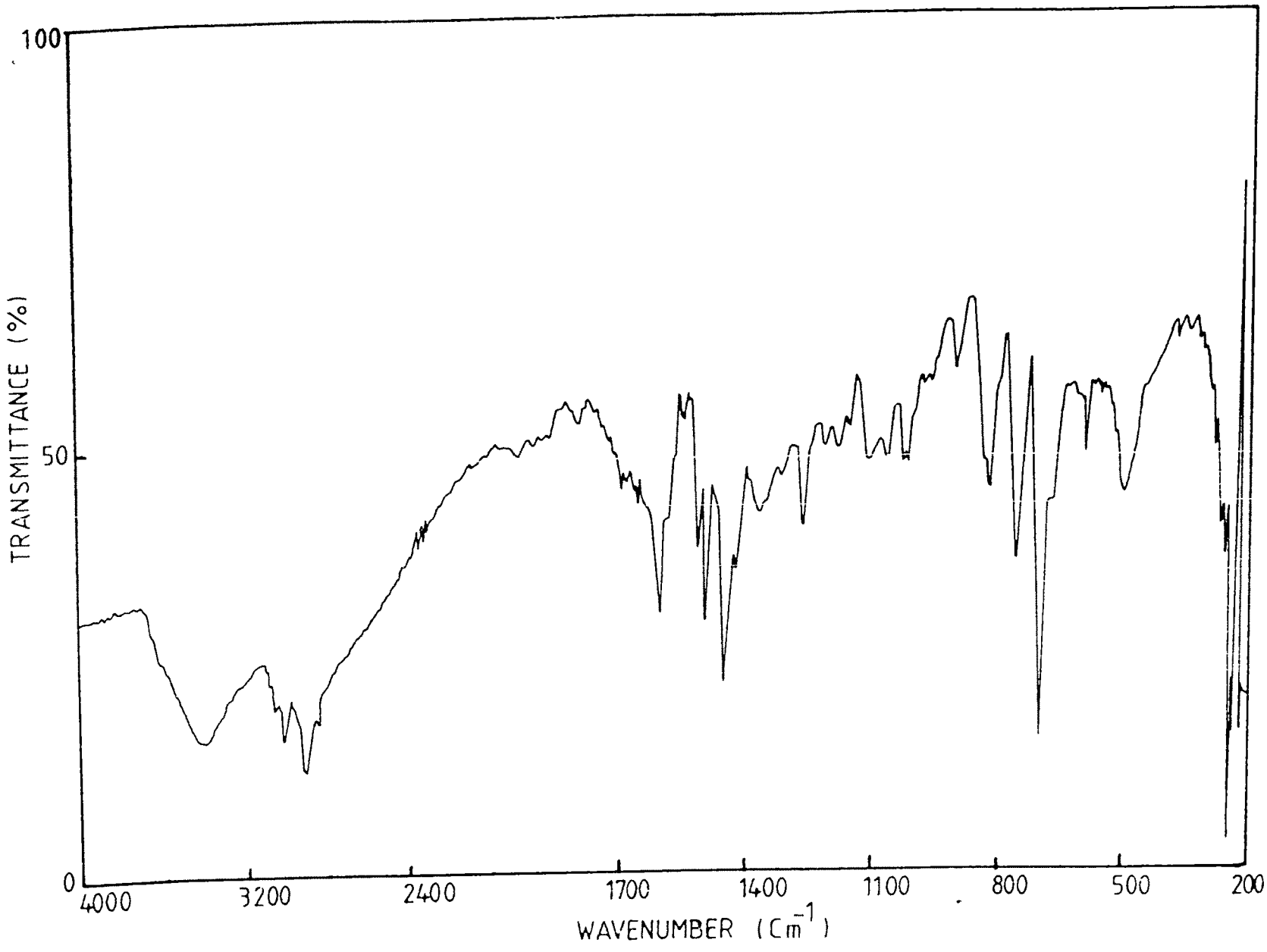

Figure-3.8 Infrared spectrum of 10PRu(III)TMDA

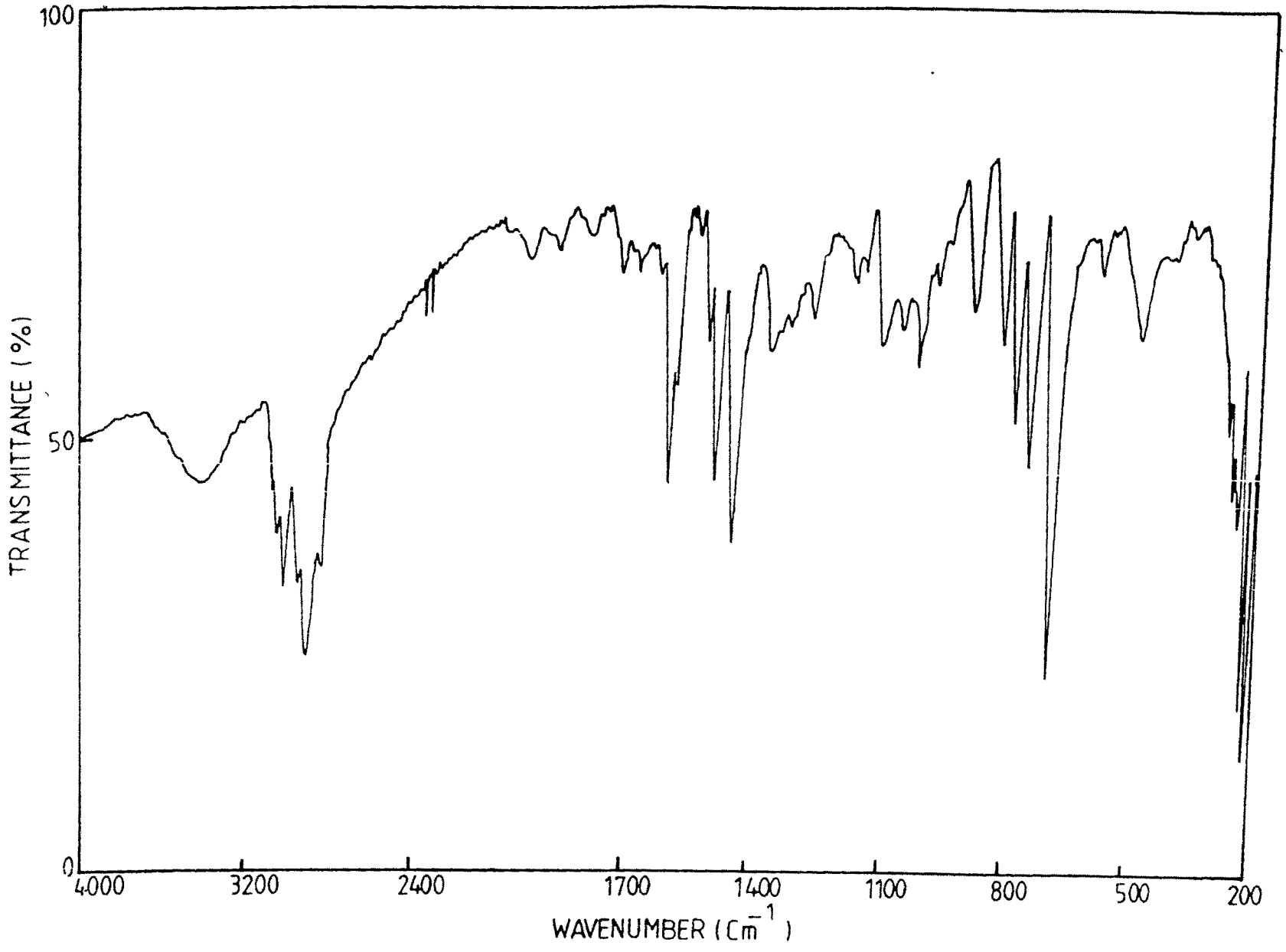

Figure-3.9 Infrared spectrum of 30PRu(III)TMDA

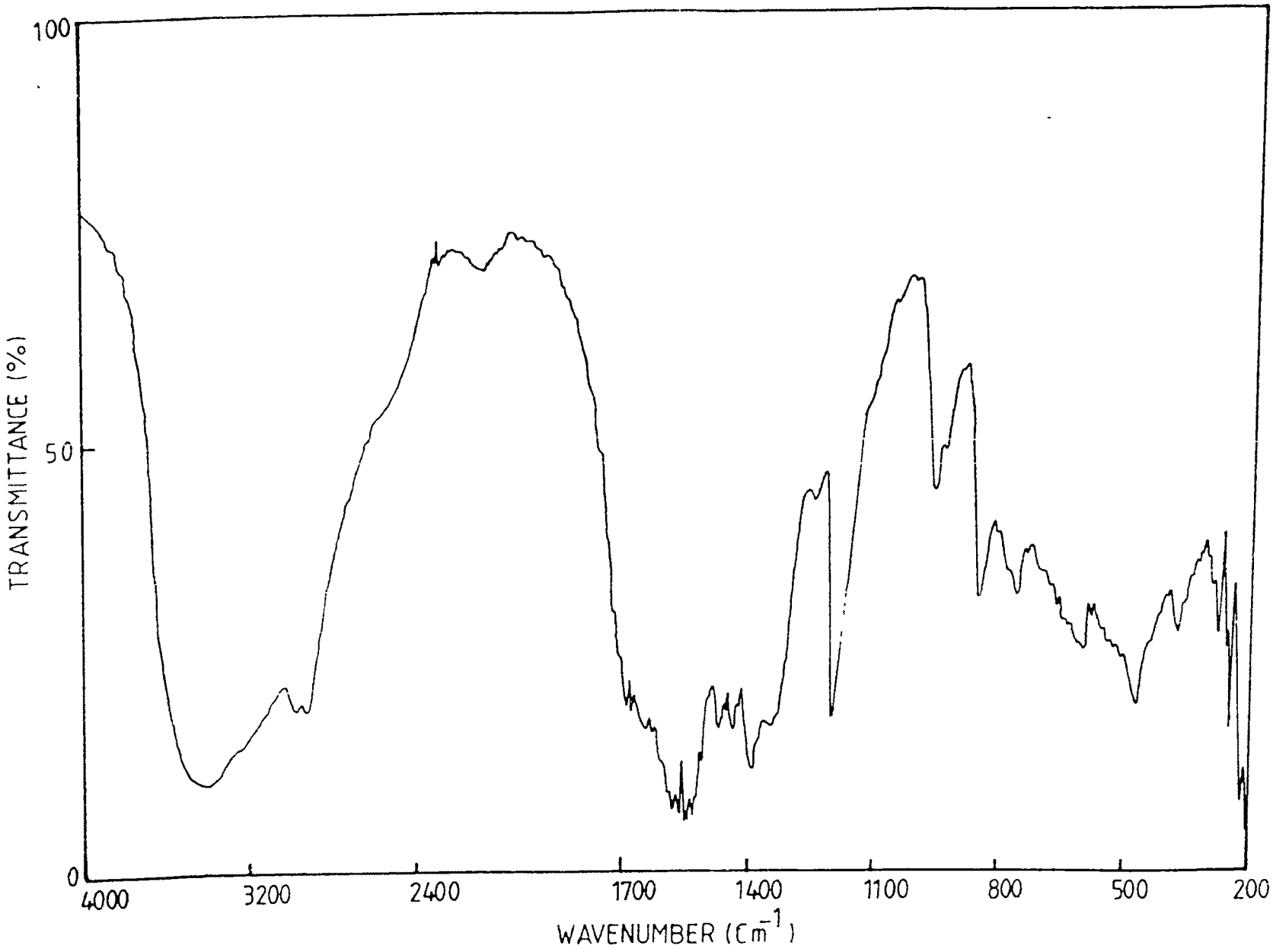

Figure-3.10 Infrared spectrum of 2.5ZKRu(III)TMDA

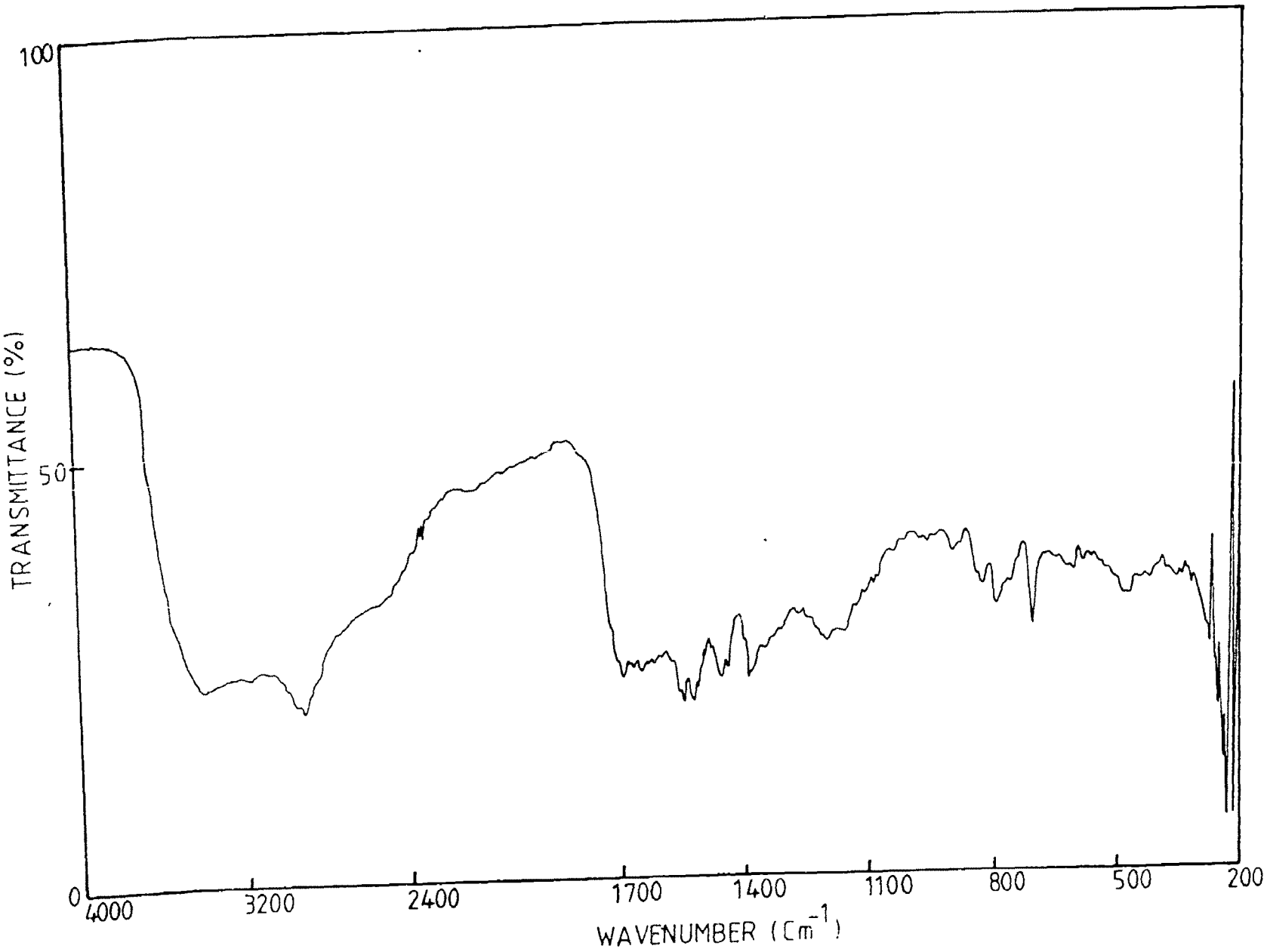

Figure-3.11 Infrared spectrum of 20ZKRu(III)TMDA

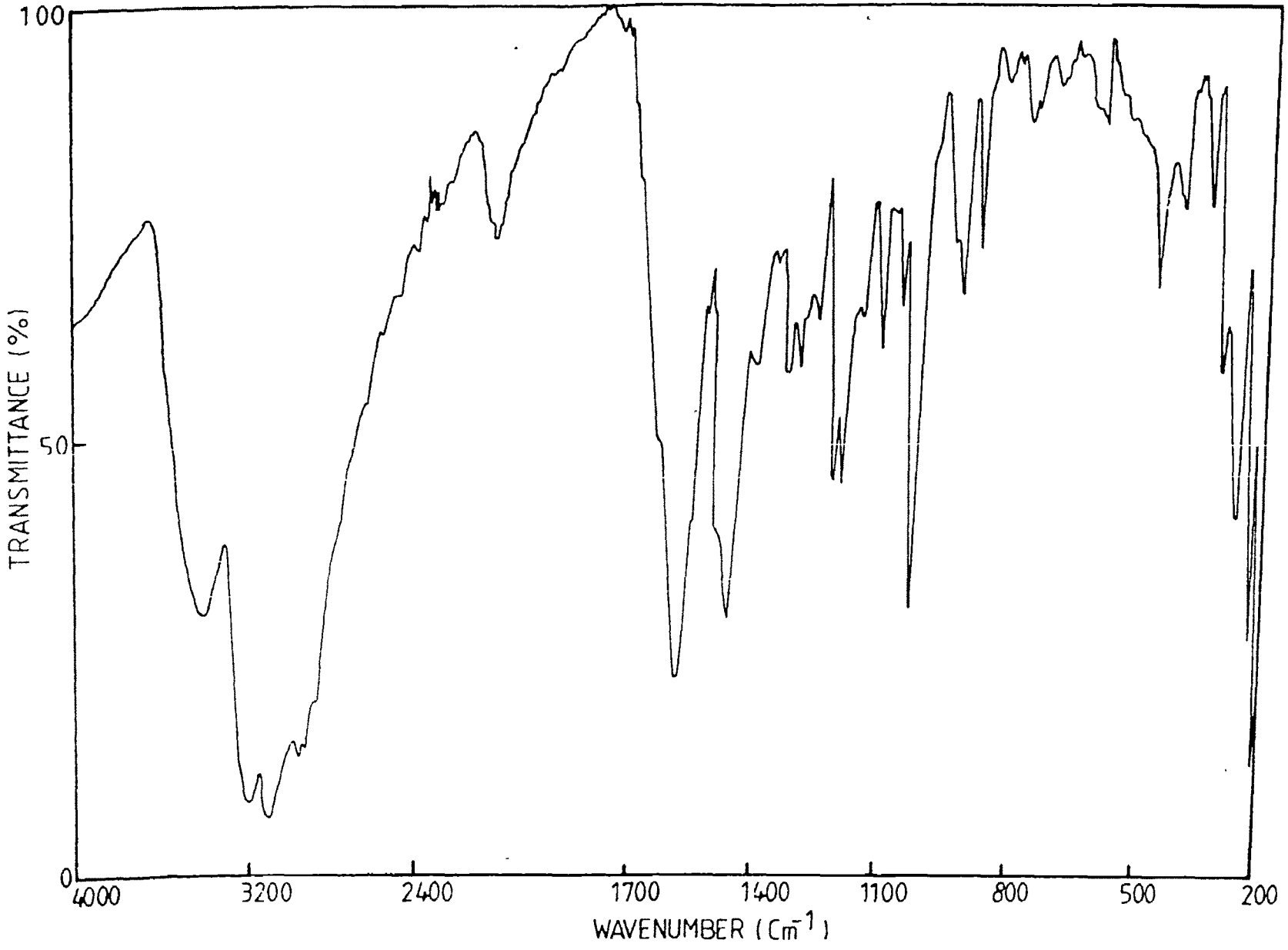

Figure-3.12 Infrared spectrum of unbound ruthenium-TMDA complex.

Table-3.7

A summary of the IR frequency assignment for polymer bound and unbound complexes

Catalyst	Ru-Cl str(Cm^{-1})	Ru-N str(Cm^{-1})	C-N str(Cm^{-1})	N-H str(Cm^{-1})	$-CH_2Cl$ str(Cm^{-1})	C=O/-OH str(Cm^{-1})
Unbound $[RuTMDACl_2]Cl$	270	380 340	1051	3429 1585	-	-
3PRuTMDA	275	385 355	1071	3419 1604	1266	-
10PRuTMDA	280	379 349	1068	3420 1603	1266	-
30PRuTMDA	277	385 350	1066	3447 1603	1271	-
2.5ZKRuTMDA	283	383 355	1226	1566	1250	1692/3400
20 ZKRuTDMA	276	390 355	1226	1547	1250	1698/3400

3.6.3 X-Ray diffraction

Since polymer-bound metal complexes are very often amorphous, few reports ~~are there~~ exist concerning x-ray analysis. The chelate complex of poly(o-isophthaloyl-isophthalamide oxime) with Cu(II) was studied by x-ray diffraction (15). Similar structure of polymer ligand as well as the chelated polymer has been suggested, and the interplanar distances of the polymer chain increased somewhat upon the reaction with Cu(II) ions. It is sometimes difficult to study the coordination structure of polymer-metal complex because of noncrystallinity. However, the extended x-ray absorption fine structure (EXAFS) has been used recently to determine the inter atomic distances and coordination of polymer-bound catalyst (16).

In the present investigation, the diffractograms of polymer-bound complexes (Figure 3.13, 3.14) indicate that poly(Sty-DVB) bound ruthenium complexes are more crystalline than Zeo-Karb bound ruthenium complexes. The percent crystallinity increases with increase in degree of crosslinking of polymer support. This is probably due to, more number of metal complex present on the surface than in the bulk in case of high crosslinked polymer support. In the case of the low crosslinked polymer the distribution of metal complex may be more in the bulk of the polymer matrix which are seen only in the swollen state.

3.6.4 Electron spectroscopy for chemical analysis (ESCA)

During the last two decades, electron spectroscopy has found several applications in chemistry. The pioneering work of Siegbhan and his co-workers (17) in high resolution electron spectroscopy resulted in a technique

Figure-3.13 X-ray spectra of 1) 3P 2) 3PRuTMDA 3) 10P
4) 10PRuTMDA

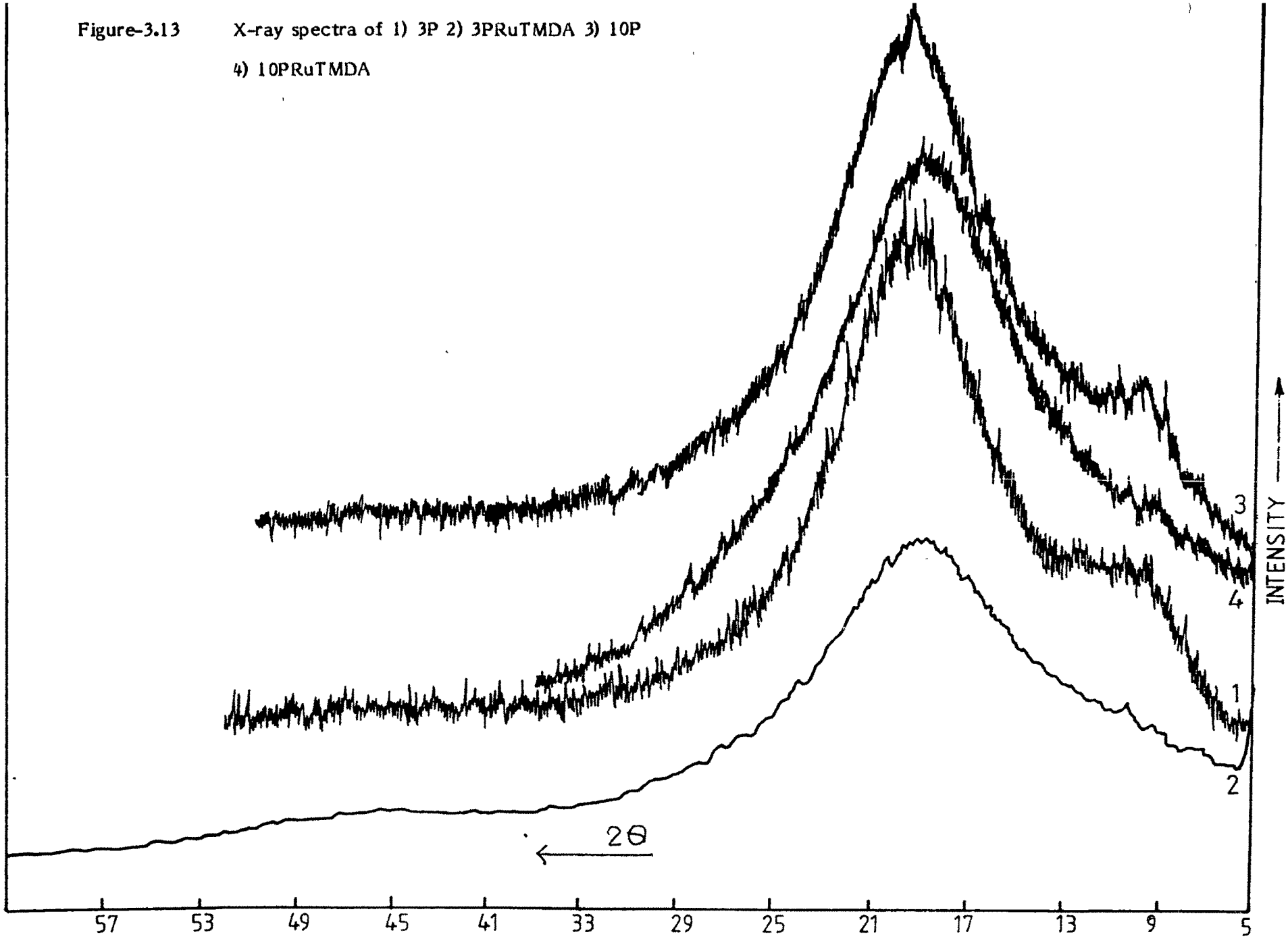

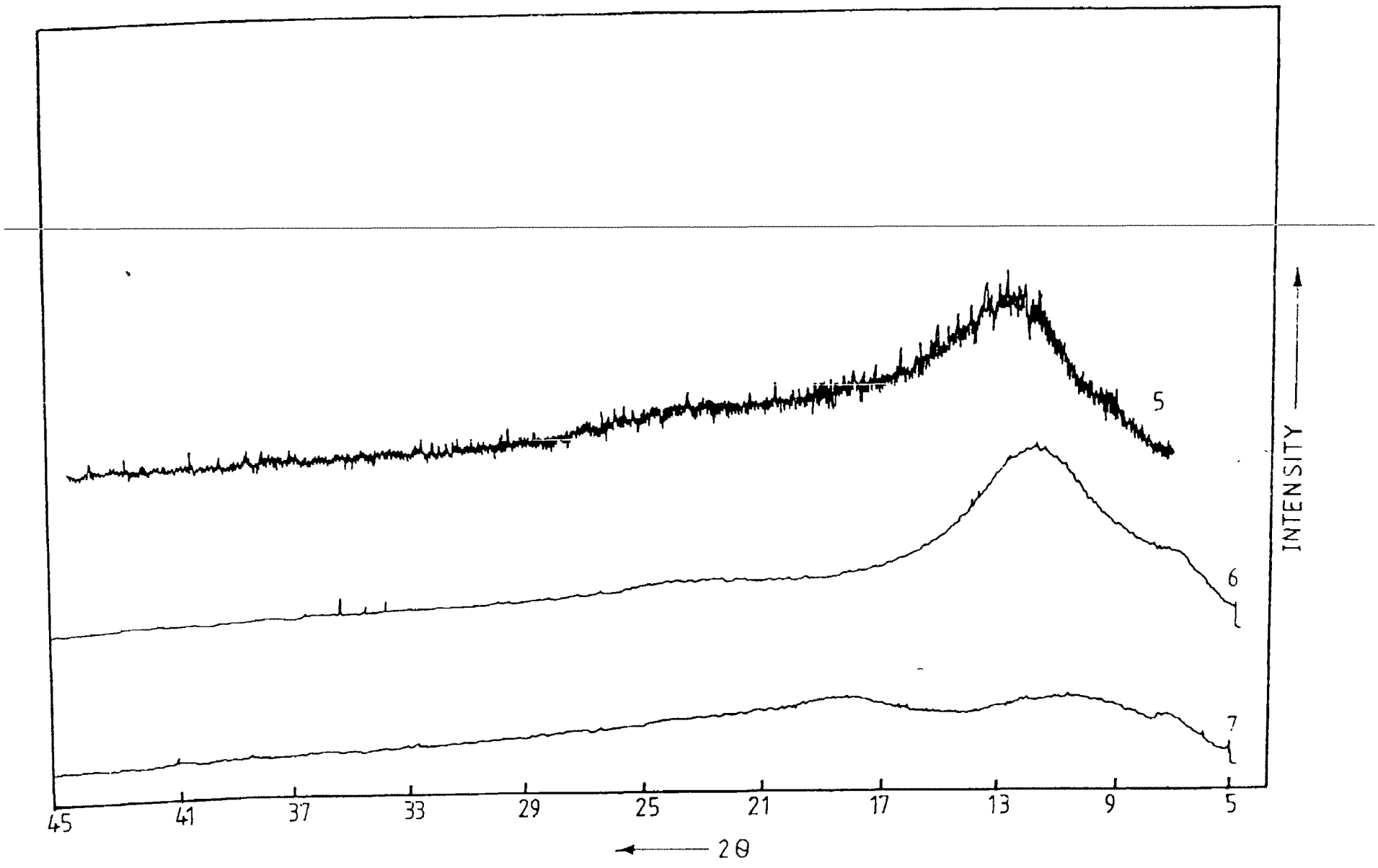

Figure-3.14 X-ray spectra of 5) 20ZKRuTMDA 6) 30PRuTMDA 7) 2.5ZKRuTMDA

which they named electron spectroscopy for chemical analysis (ESCA). In ESCA, a specimen is irradiated by soft x-ray and the resulting photo-electrons are dispersed through either a magnetic field or an electrostatic field. Due to the high resolution available with the electron spectrometers, kinetic energies can be very accurately obtained which in turn will provide accurate data on binding energies of the core electrons. Since binding energy of the core electron is a finger print of the atom, ESCA provides rapid elemental analysis. One can also get information regarding the chemical state of an element from ESCA, due to the so-called 'chemical shift' observed in the photoelectron spectrum. This aspect of ESCA is particularly responsible for its extensive use in catalysis (17).

ESCA study of polymer bound ruthenium catalyst (Figure-3.15 (a,b)) showed peaks due to Ru(3d 3/2), Ru(3p 3/2), N (1s), Cl (2p 3/2) and C (1s) for ruthenium-TMDA, indicating that the ruthenium is present in +3 oxidation state. The broadening and shift of ESCA lines may be due to the different chemical environment of the polymer bound ruthenium complex (18). The intensity reversal is due to the superposition (19) of C (1s) peak with the Ru(3d 3/2).

3.65 Electron paramagnetic resonance (EPR)

The electron paramagnetic resonance has been found to be a very powerful spectroscopic tool for investigating a variety of physico-chemical problem, especially when system under investigation contained a paramagnetic species. For conducting EPR investigations, a suitable paramagnetic probe, either intrinsic or extrinsic, should form a part of the system and this probe should not preferably perturb the environment. Under these conditions, the EPR spectrum of the probe gives information about the

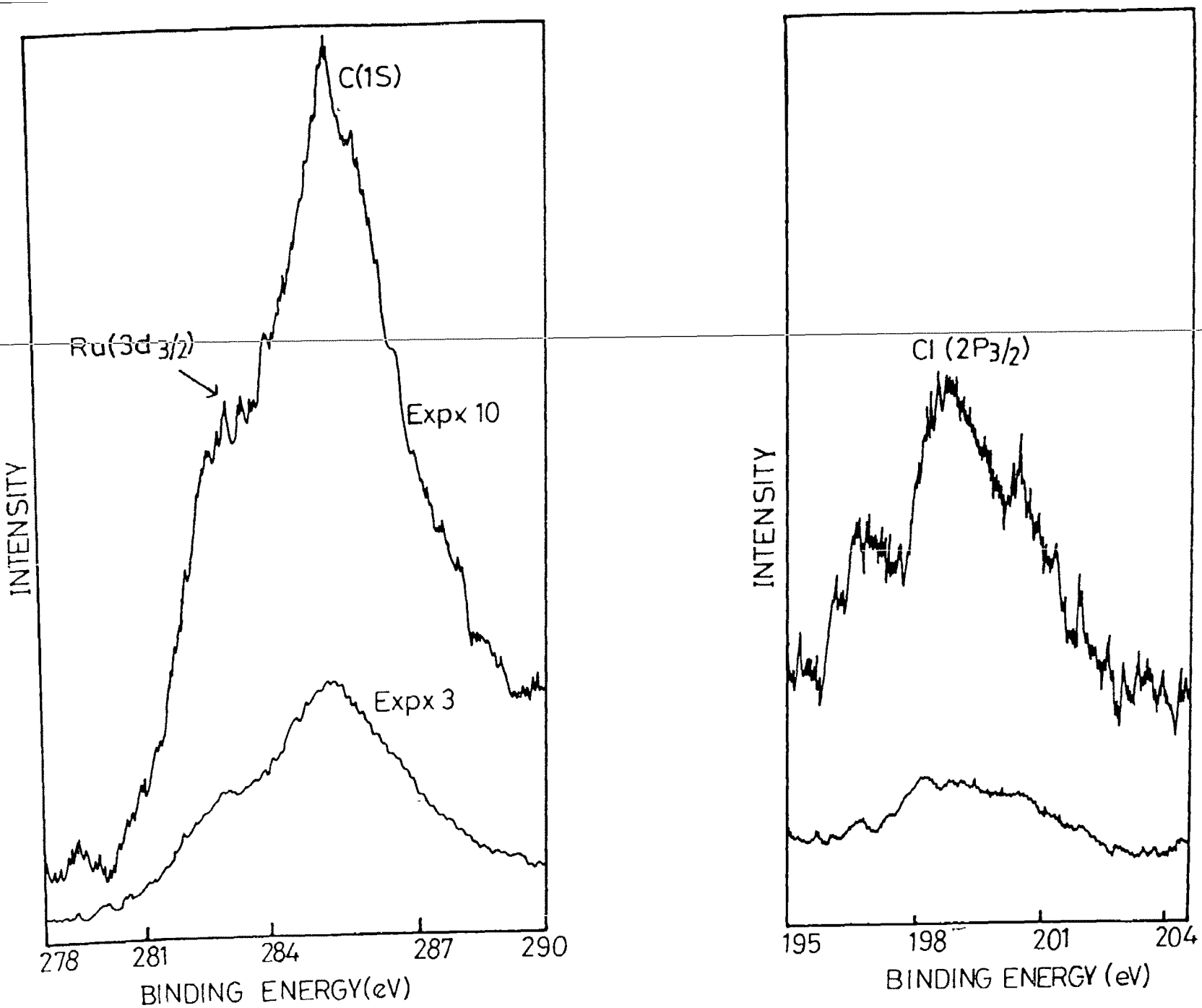

Figure-3.15(a) ESCA spectra of 30PRu(III)TMDA

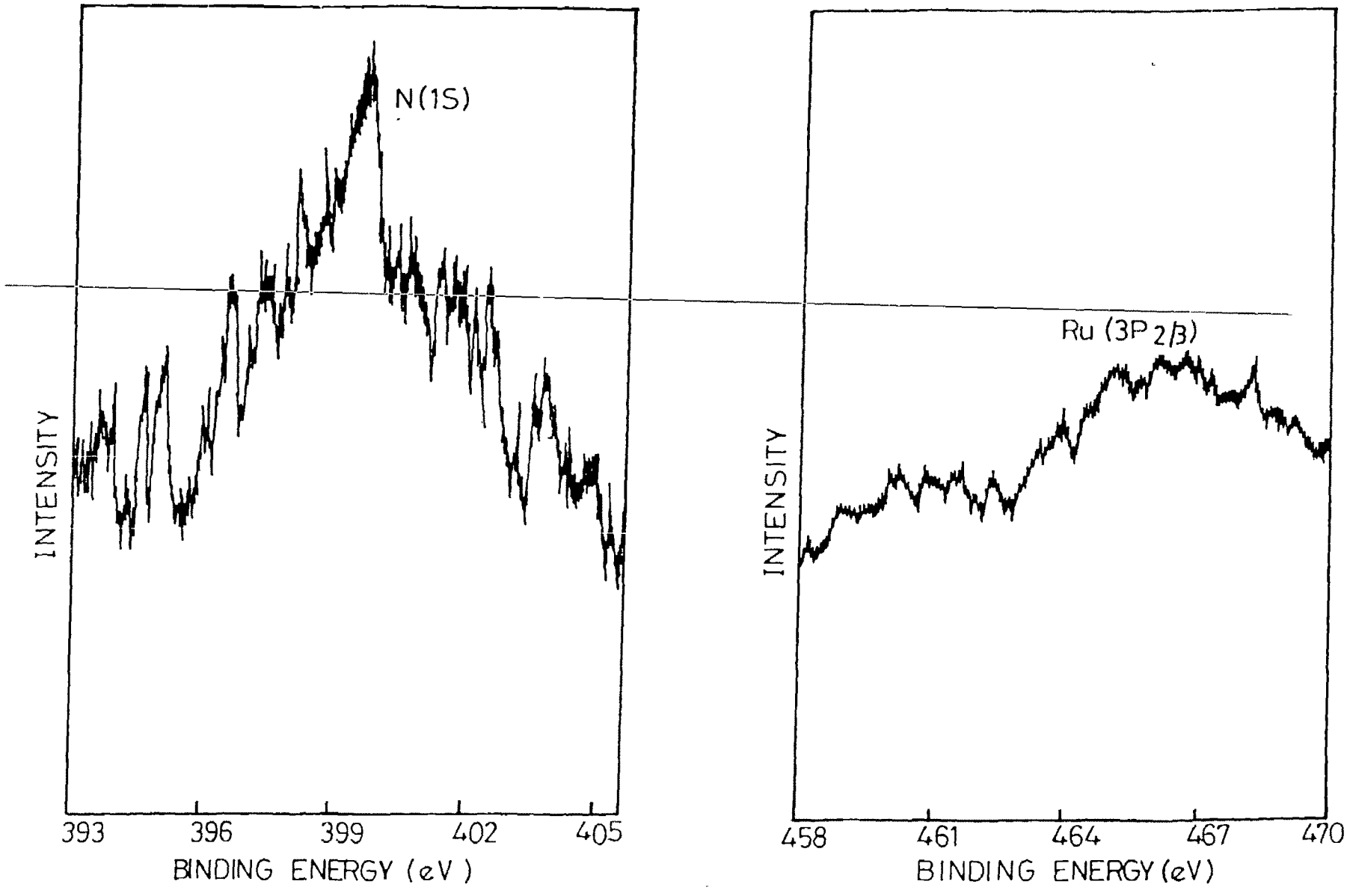

Figure-3.15(b) ESCA spectra of 30PRu(III) TMDA

nature of chemical bonding, electron-nuclear hyperfine interactions, site symmetries and temperature or pressure induced changes therein, reaction intermediates etc. Therefore, this technique finds wide applicability in the study of paramagnetic defects that exist on solid surfaces such as adsorbed molecules or radical ions, metal ions of d or f-block elements and intrinsic surface defects. The identification of the surface species has to be preceded by information on the well characterized EPR spectrum of the species of interest in bulk (16).

EPR has been extensively applied in the investigation of physico-chemical properties of 3d and 4d electron system. Among these, d^1 (Ti^{3+}, V^{4+}, Mo^{5+}), d^3 (V^{2+}, Cr^{3+}), d^5 (Mn^{2+}, Fe^{3+}, Cr^{+}), d^7 (Co^{2+}, Pd^{3+}, Rh^{2+} in low spin form) and d^9 (Cu^{2+}, Pd^{+}) electron systems have been most exhaustively studied and these studies have wide range of applications including in surface science and catalysis as the ions with these configuration give EPR spectrum over a wide range of temperatures (20).

EPR is essentially due to transitions between two energy levels of an unpaired electron, corresponding to two spin states in the presence of an external magnetic field. For a free electron, which is not interacting with surroundings, the transition energy is given by

$$\nu h = \Delta E = g_e H \beta$$

where h is the Plancks constant, ν is the microwave frequency, β is the Bohr magneton, H is the strength of the external magnetic field and g_e is the free electron g-value equal to 2.0023. In the complexes g_e varies from the free electron according to the electronic environment in the molecule.

EPR spectrum of homogeneous catalyst, [Ru(III)TMDACL$_2$]Cl is shown in Figure-3.16. The $g_\perp$ and $g_{||}$ values were found to be 1.994 and 2.424, and g_{av} is 2.28. This is in accordance with a low spin d^3 centre in square planer environment, i.e. ruthenium is present in low-spin +3 oxidation state. Since the spectrum does not resemble a triplet state spectrum the possibility of Ru being in +4 oxidation state can be ruled out (low-spin Ru(IV) will have two unpaired electrons). The possibility of Ru(II) may also be eliminated because it is diamagnetic and hence EPR inactive. Similar results have been reported by other workers for Ru(III) carbonyl complexes (21-23). Taqui Khan et al. have studied the EPR spectrum of Ru(III) carbonylchelates of schiff bases and average g value was obtained to be 2.1 confirming the presence of ruthenium in +3 oxidation state (24).

Higher value of $g_\perp$ than the $g_{||}$ indicates that the ligand field in xy plane is stronger. In the present case this is possible only if the complex has following structure.

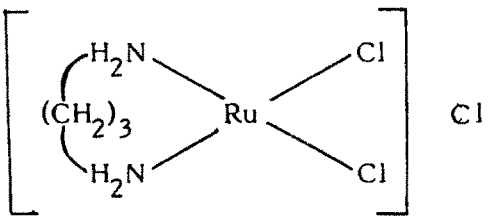

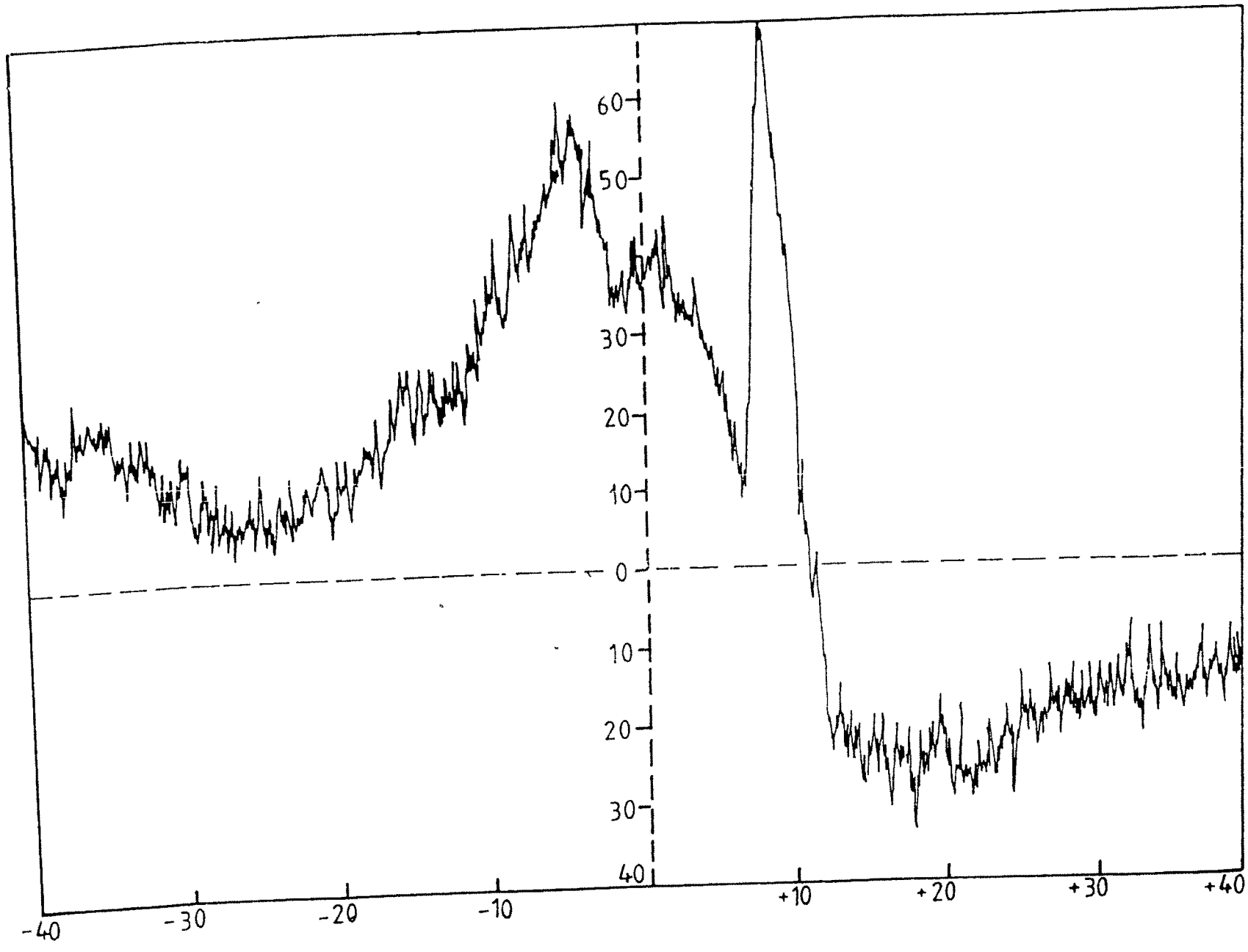

Figure-3.16 EPR spectrum of homogeneous catalyst, $[RuTMDACl_2]Cl$

3.7 Morphology of polymer supports and polymer bound catalyst

Many practical catalysts have a complex geometric structure and their catalysing surface consist of a complex chemical mixture of different phases. The active component is frequently in the form of very small crystals dispersed on the large surface area of a spongy supporting component of the catalysts. The behaviour of the catalyst depends upon the structure and composition of the active component as well as the morphology of its supporting medium. It can be determined on the basis of its structure at a range of magnification (from a few hundred to a few millions times) which gives the information about the nature and the distribution of the active components, the nature of the porosity etc. The magnification in the simple electron microscopy is limited, an extension of magnification by several order of magnitude is obtained with scanning electron microscope (SEM). This can be made in order to study the morphology of the catalysts (25).

Scanning electron micrographs of supports and catalysts are presented in plates 3.1-3.3 respectively.

Comparison of micrographs of supports (plates 3.1, 3.2) shows that, mostly polymer beads are spherical, porous and the texture changes with the change in the digree of crosslinking of polymer.

Striking changes are noticed in porous texture of the polymer supports after loading the metal complexes. A change in the shape of polymer beads has been found after anchoring the metal complexes. These changes are also revealed in the surface area measurements.

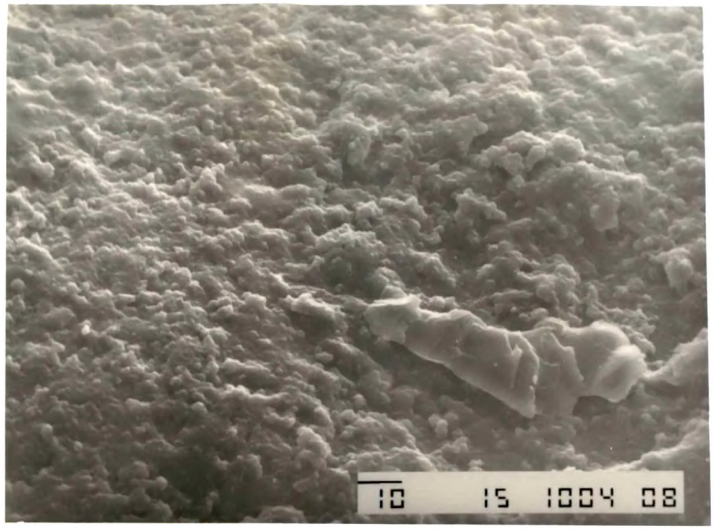

3P 700X

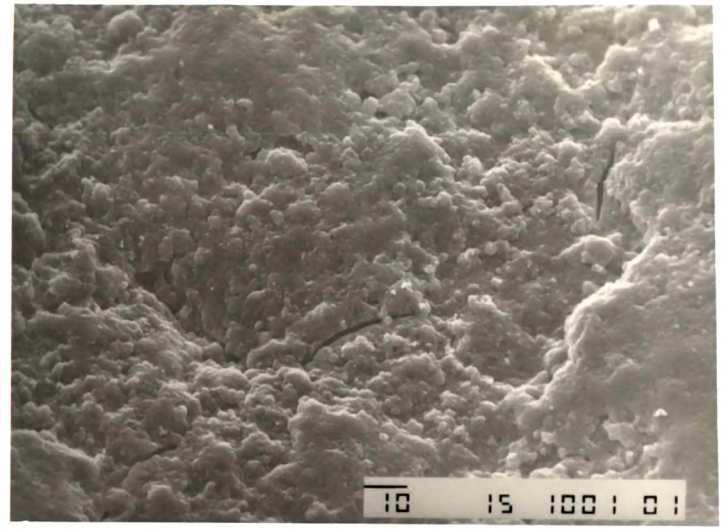

3PRuTMDA 750X

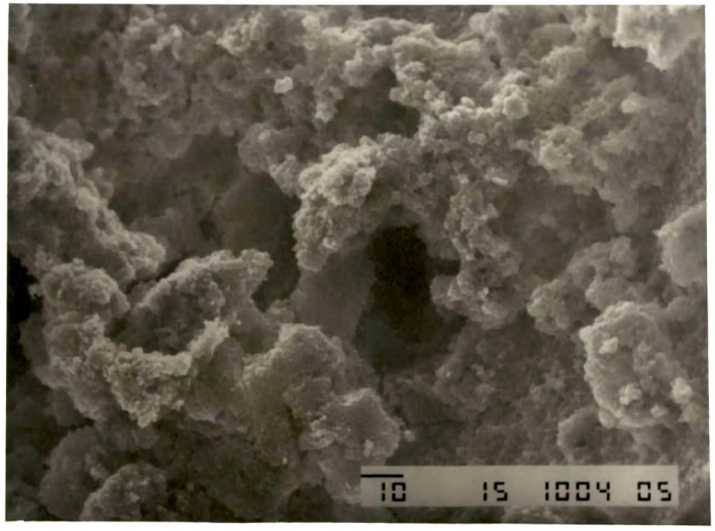

10P 750X

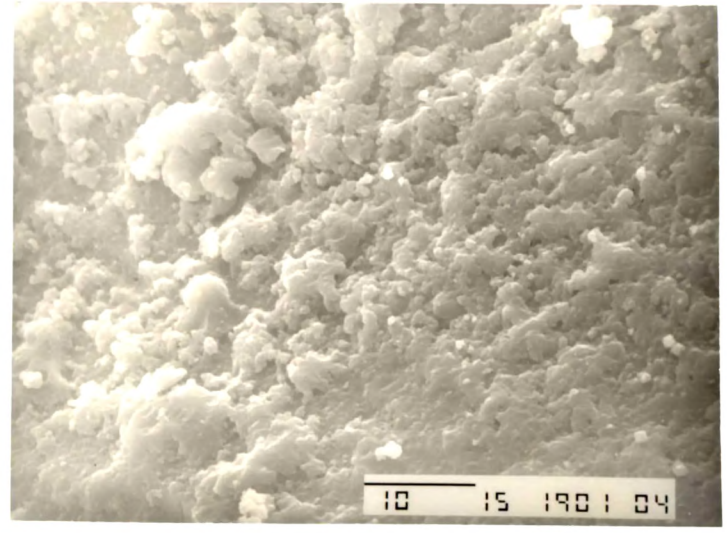

10PRuTMDA 1600X

Plate 3.1 Scanning Electron Micrographs of Polymer Support and Catalyst.

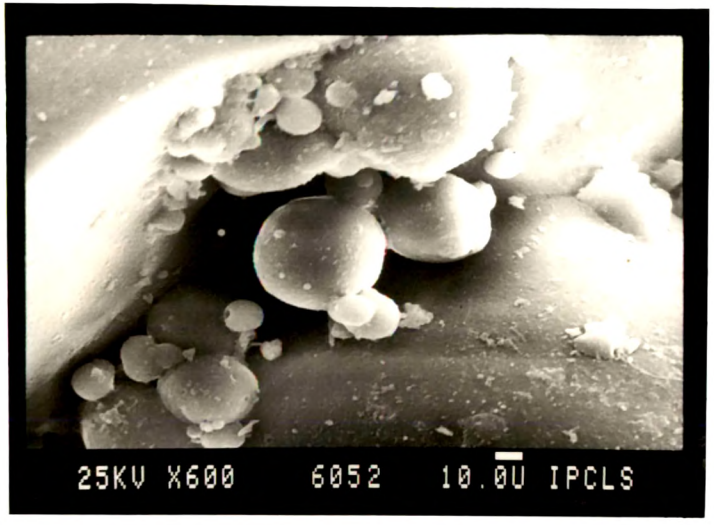

30P 600X

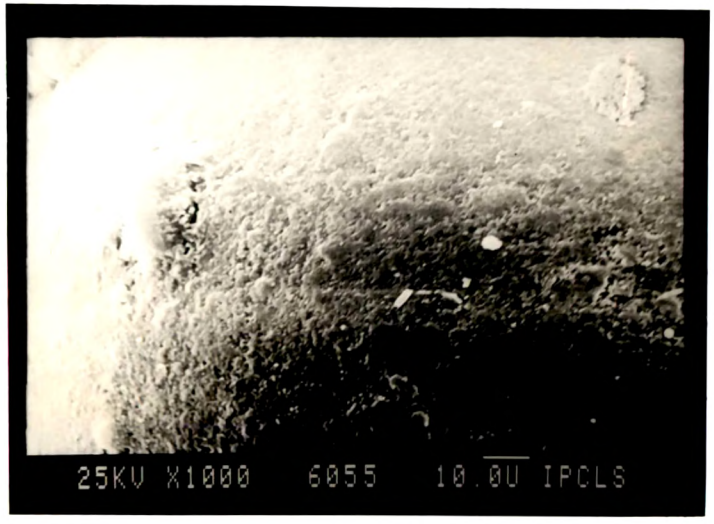

30PRuTMDA 1000X

Plate 3.2 Scanning Electron Micrographs of Polymer Support and Catalyst.

2.5 ZK 600 X

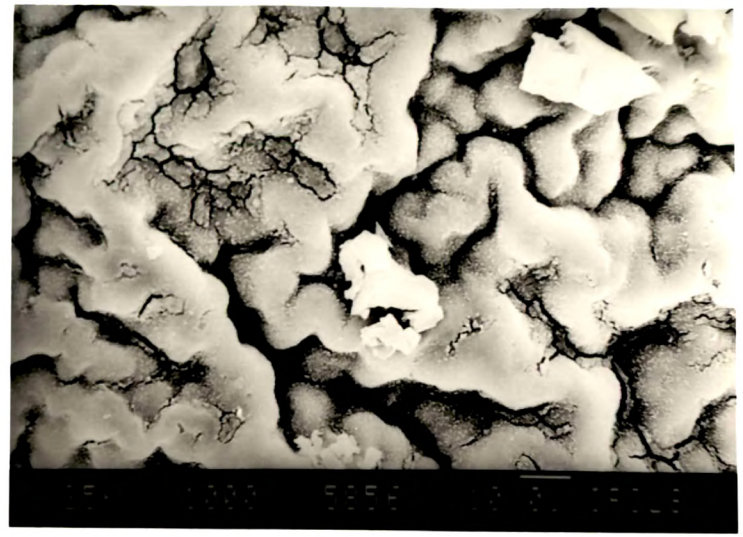

2.5ZKRuTMDA 1000X

20ZK 4000 X

20ZKRuTMDA 1500 X

Plate 3.3 Scanning Electron Micrographs of Polymer Support and Catalyst.

3.8 Thermal stability

The change in weight and thermal property of a catalyst with changing experimental conditions can be used for a variety of studies. In the case of polymer bound metal complex catalysts, weight loss or heat change may reveal the stability and phase change as a function of environment.

The thermal stability of many ruthenium and rhodium complex catalysts (26-29) was found to be enhanced when supported on the solid material (i.e. inorganic oxides or polymers). Since the thermal properties, along with the other properties of polymer support varies with the crosslinking of the polymer, the microenvironment around metal ion changes coordination sphere of the metal ion, induced by complex formation on the polymer matrix, which further leads to special stability of metal complex. Thus comparative study of the thermal behaviour of polymer support, unbound metal complex and polymer bound metal complex will be useful to limit the catalytic reaction temperature.

3.8.1 Thermal stability of the support

Figure-3.17 shows the TGA of poly(Sty-DVB) support used for the synthesis of the catalyst. It is clear from the figure that polymer supports prepared are hydrophobic, thermally stable upto 150°C and polymer degradation starts above 200°C. Therefore the supports can be used very safely upto 100°C

In order to investigate the thermal stability of the support, a separate experiment was carried out. The supports were isothermally heated at 175°C

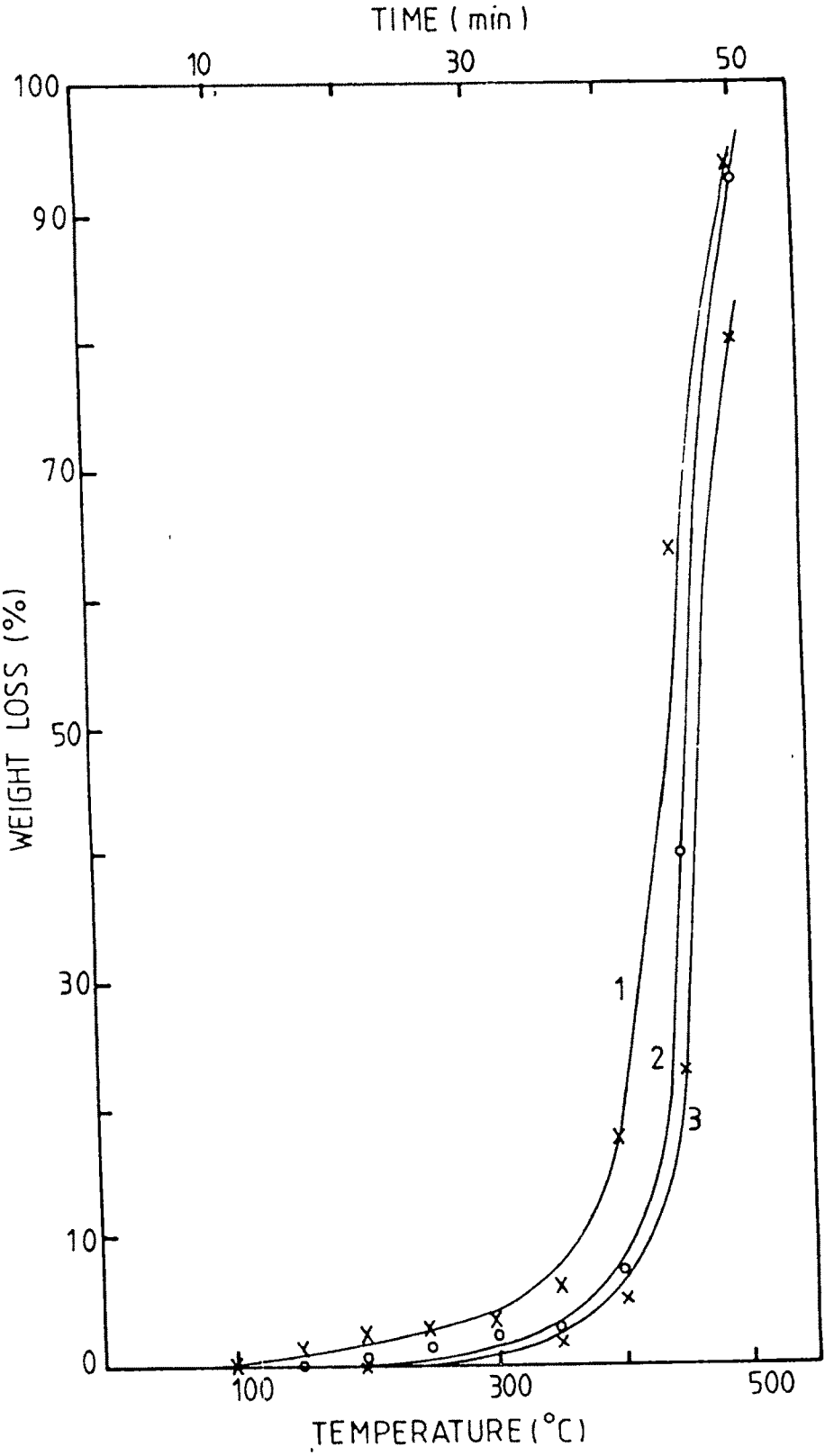

Figure-3.17 Thermogravimetric curves of polymer supports 1) 3P 2) 10P 3) 30P

for a period of 5 hours (Figure - 3.18). It was noticed that in the case of 3% crosslinking, degradation occurs to a lesser extent (i.e. 6 wt%) and in the case of 10% crosslinking, degradation occurs upto 8% weight loss within 5 hours, after which the polymer is stable. This loss may be due to degradation of polymer upto some extent, or due to the evaporation of organic matter entrapped inside the fine pores. Whereas in the case of 30% crosslinking, only 1% degradation occurs.

Similar observation was found from the morphology of support after heating isothermally at 175°C for 5 hours (plate 3.4). Hence it was ensured that the polymer-anchored catalysts can be used in catalytic studies below 150°C.

3.8.2 Thermal stability of catalysts

Figure-3.19 shows the DTA and TG curves for unbound ruthenium complex. It may be noted that metal complex is stable upto ~ 200°C. Above this temperature metal complex changes its phase. ~~That it~~ which is reflected from endothermic DTA peaks. Initial weight loss is due to moisture.

TGA curves for poly(Sty-DVB) bound ruthenium complexes are shown in Figure 3.20. It is observed that thermal stability of polymer-supported catalyst is comparable with that of the support used.

Figure-3.21 shows the TGA of the Zeo-Karb resin and Zeo-Karb supported ruthenium complex. It is clear from the figure that polymer after supporting ruthenium complex undergoes some change.

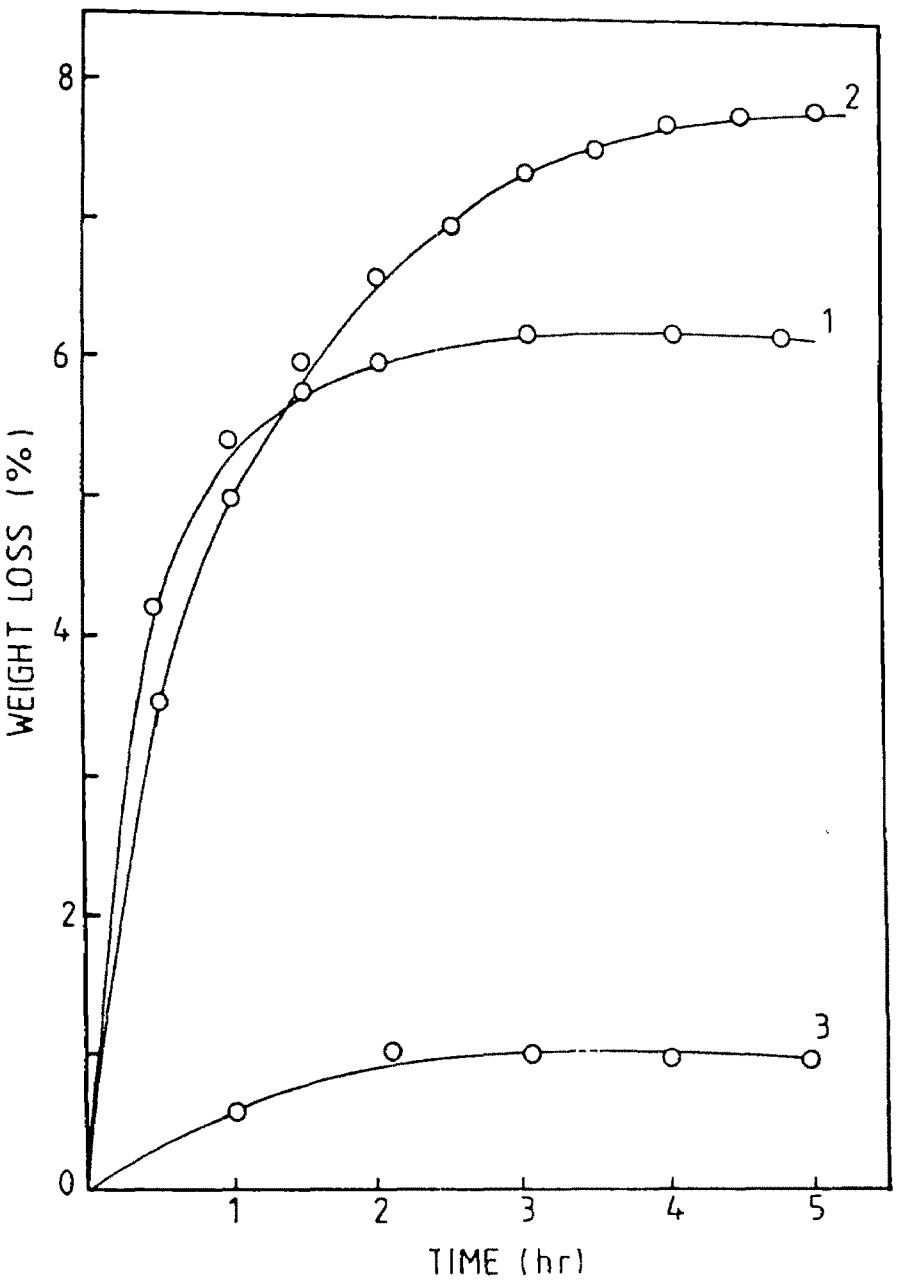

Figure-3.18 Thermogravimetric curves of polymer supports 1) 3P 2) 10P 3) 30P

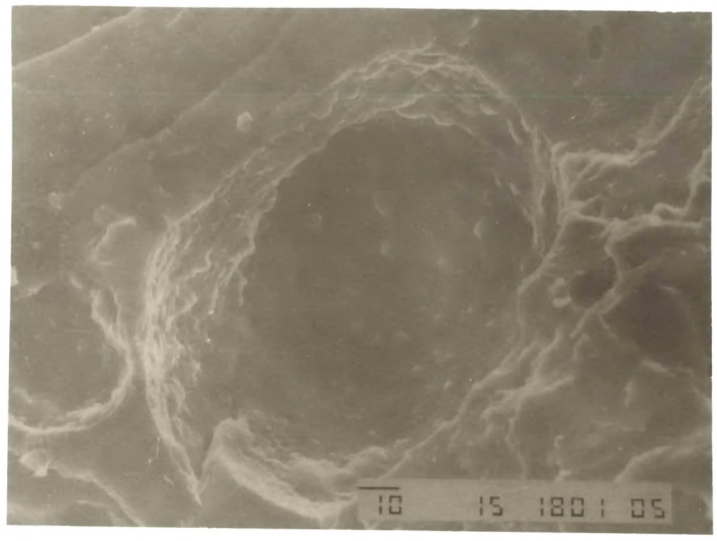

3P 700X

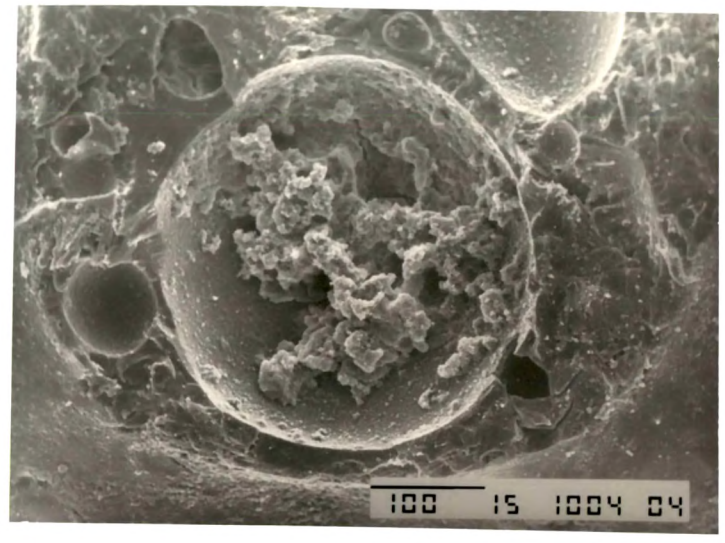

10P 1200X

20ZK 1500X

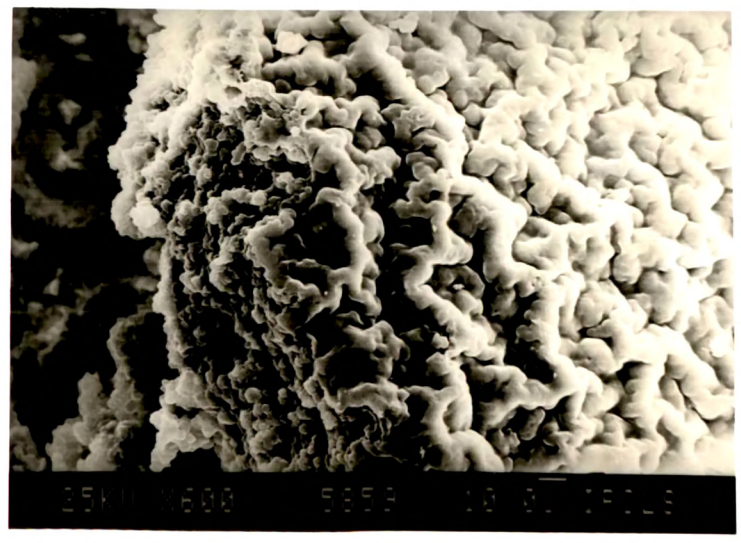

2.5ZK 600X

Plate 3.4 Scanning Electron Micrographs of Polymer Support.

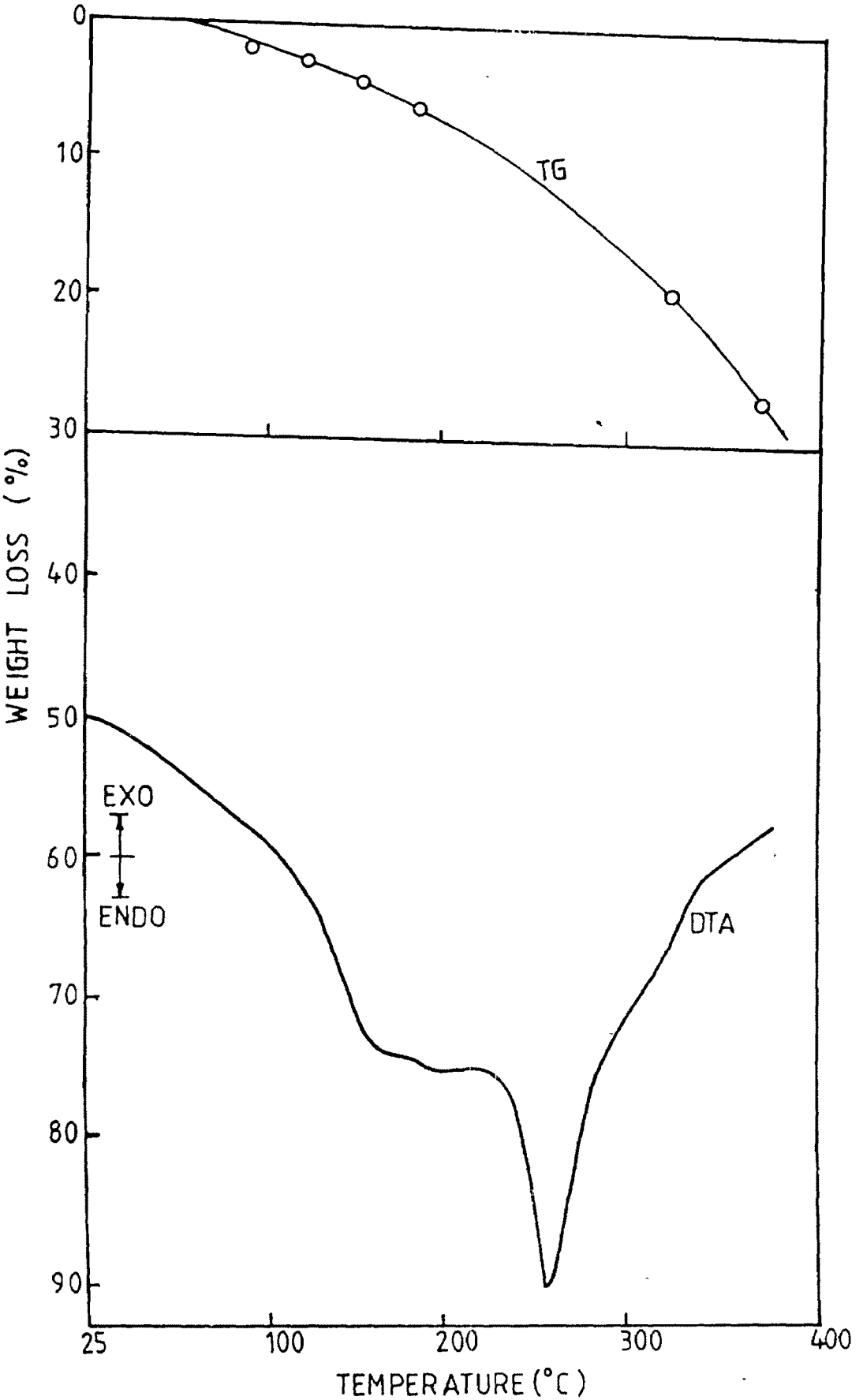

Figure-3.19 DTA/TG curves of unbound ruthenium-TMDA complex.

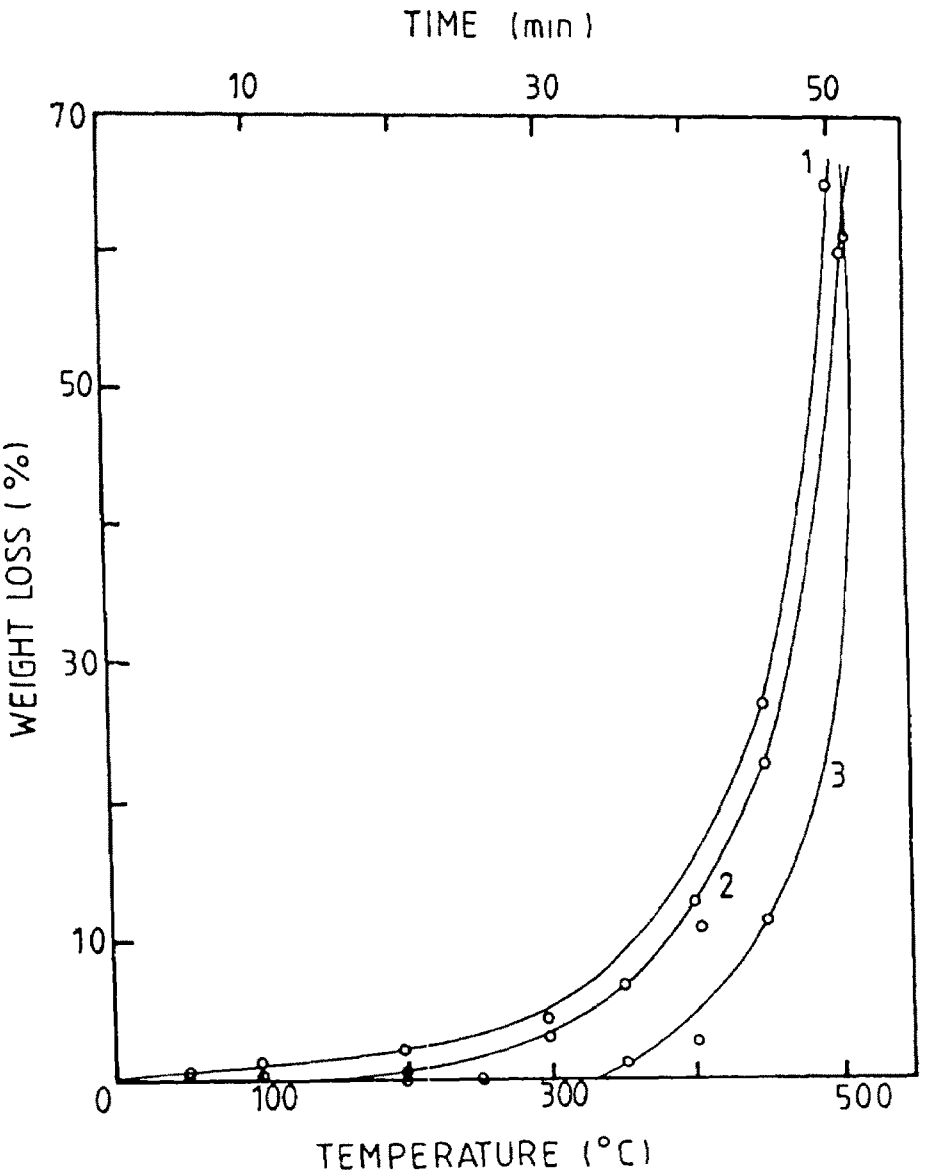

Figure-3.20 Thermogravimetric curves of polymer supported catalyst 1) 3PRuTMDA 2) 10PRuTMDA 3) 30PRuTMDA

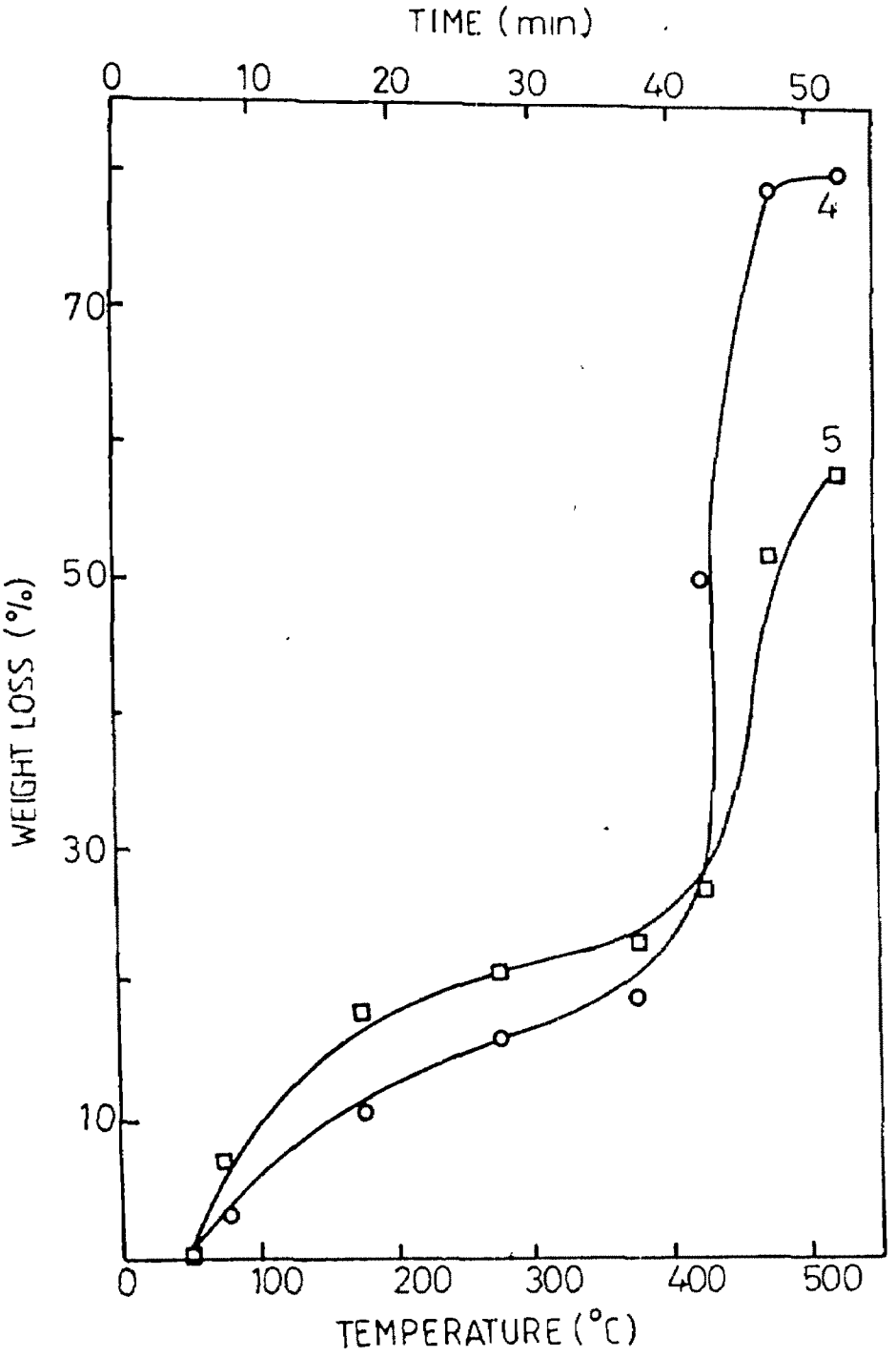

Figure-3.21 Thermogravimetric curves of 4) Zeo-Karb 226

5) 2.5ZKRuTMDA

Finally it can be concluded that all the polymer anchored catalysts in the present investigation may be employed practically safely below 100°C. The initial weight loss upto 100°C in all the cases is due to loss of moisture present in the catalysts as indicated in Table-3.1.

From all the above physicochemical characterization and spectroscopic evidence, the following possible structures for the polymer-bound catalyst have been proposed (Schemes 3.1, 3.2).

SCHEME - 31

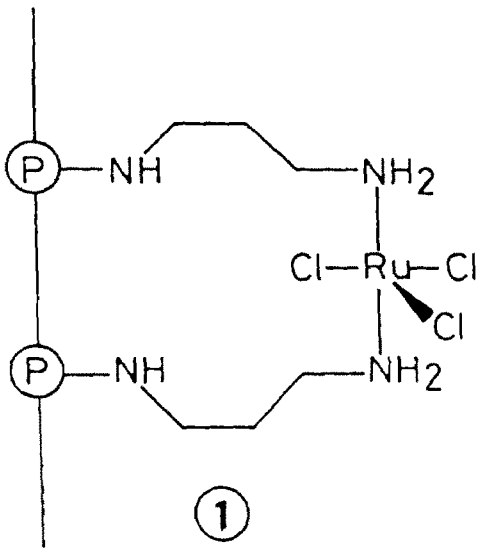

1

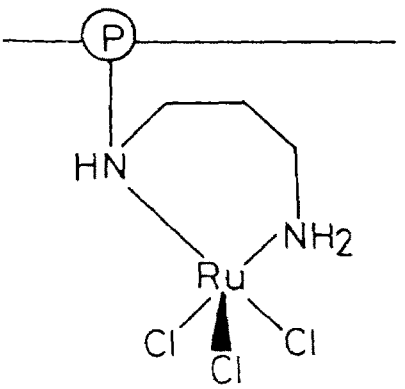

2

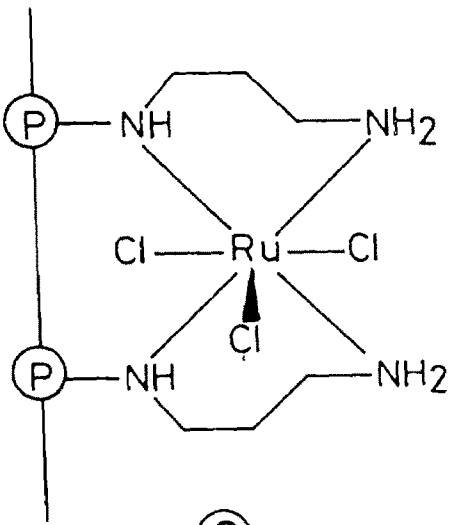

3

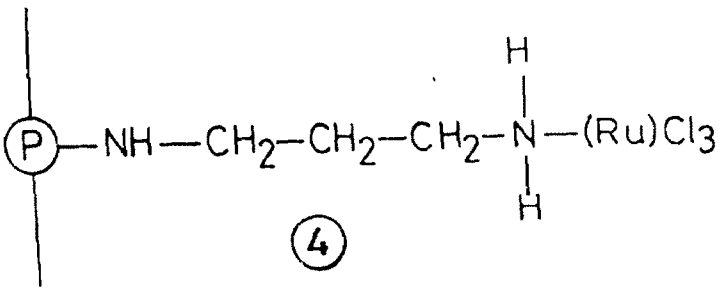

4

Where (P) = copolymer of styrene-divinylbenzene

SCHEME– 3.2

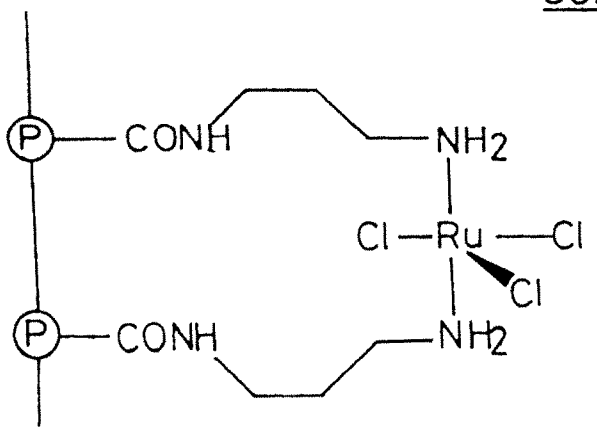

1

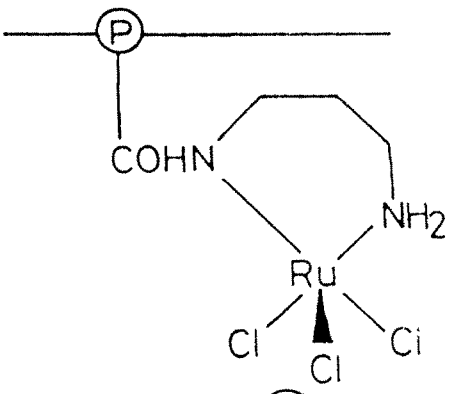

2

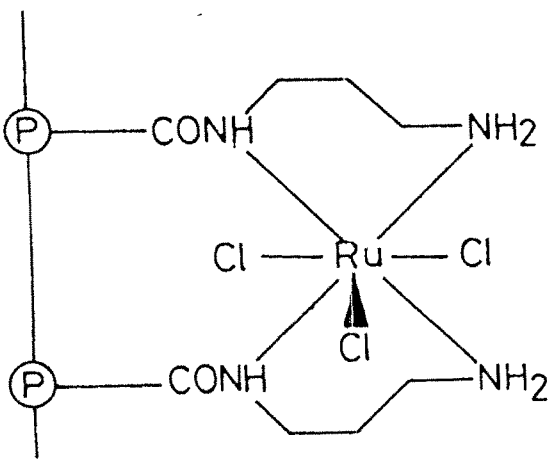

3

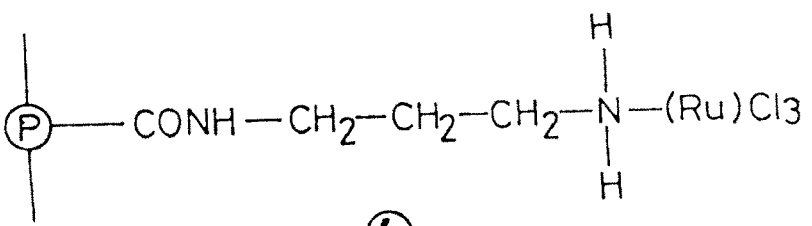

4

Where (P) = Zeo-Karb 226 resin

3.9 References

1. R. Kunin, "Ion Exchange Resins"; John Wiley and Sons Ltd. (1958).
2. S. Bhaduri and Hanif Khwaja; J. Chem. Soc. Dalton Trans; 415 (1983).
3. D. M. Young and A. D. Crowell, "Physical Adsorption of Gases", Butter Worths, London (1962).
4. S. J. Gregg and K. S. W. Sing, "Adsorption, Surface Area and Porosity", Academic Press, London (1967).
5. W. W. Wendlandt and H. G. Hecht, "Reflectance Spectroscopy"; Wiley Inter. Sci, New York (1966).
6. G. Kortum, "Reflectance Spectroscopy, Principles, Methods, and Application"; Springer-Verlag, Berlin (1969).
7. K. Klier; Catal. Rev. ; 1, 207 (1967).
8. W. N. Delgass,. G. L. Haller, R. Kellerman and J. H. Lunsford, "Spectroscopy in Heterogeneous Catalysis", Chapter-4, Academic Press, New York (1979).
9. Y. Kurimura, E. Isuchida and M. Kaneko; J. Polym. Sci; A(I), 9, 3521 (1971).
10. J. Roda; Makromol. Chem; 178, 203 (1977.
11. C. K. Poon and C-M. Che; J. Chem. Soc. Dalton Trans; 756 (1980).
12. K. Nakamoto," Spectra of Inorganic and Coordination Compounds 3rd edn.", Wiley, New York (1978).
13. E. Seddon and K. Seddon," The Chemistry of Ruthenium"; Elsevier, Amsterdam (1984).
14. A. B. P. Lever, "Inorganic Electronic Spectroscopy"; Elsevier, Amsterdam (1987).

15. A. Lehtinen, S. Purokoski and J. J. Lindberg; Makromol. Chem.;176, 1553 (1975).

16. J. Reed, P. Eisenberger, B. K. Teo and B. M. Kincaid; J. Amer. Chem. Soc., 100, 2375(1978).

17. P. S. Murty in "Spectroscopic Methods in Heterogeneous Catalysis", Eds. N. M. Gupta, V. B. Kartha and R. A. Rajadyaksha; Tata McGraw--Hill Publ. Co. Ltd., New Delhi, India, P-167(1991).

18. M. M. Taqui Khan, S. A. Samad and M. R. H. Siddiqui; J. Mol.Catal; 50, 97 (1989).

19. D. K. Chakrabarty, P. K. Basu, A. Patil, N. Ramachandran and P. D. Prabhawalkar; "Advances in Catalysis, Science and Technology", Ed. T. S. R. Prasada Rao; Wiley Eastern Ltd; New Delhi, India (1985).

20. M. S. sastry in "Spectroscopic Metaods in Heterogeneous Catalysis", Eds. N. M. Gupta, V. B. Kartha and R. A. Rajadhyaksha; Tata McGraw-Hill Publ. Co. Ltd., New Delhi, India, P-221 (1991).

21. A. Hudson and M. J. Kennedy; J. Chem. Soc. (A); 1169 (1969).

22. B. L. Gustafson, M-J Lin and J. H. Lunsford; J. Phys. Chem; 84, 3211 (1980).

23. S. Sakaki, Y. Yanase, N. Hagiwara, T. Takeshila, H. Naganuma, A. Ohyoshi and K. Ohkubo; J. Phys. Chem. Soc; 86, 1038 (1982).

24. M. M. Taquikhan, D. Srinivas, R.I. Kureshy and N. H. Khan; Inorg. Chem; 29, 2320 (1990).

25. J. V. Sanders in "Catalysis, Science and Technology"; Eds. J. R. Anderson and M. Boudart; Springer-verlag, Berlin, Heidelberg; Vol.7, P-51 (1985).

26. L. Jinxing, Y. Lixin, G. Shiuvying, H. Lijuan, T. Renyuan and L. Dongbai; Thermochimica Acta; 123, 121 (1988).

27. N. L. Holy in "Fundamental Research in Homogeneous Catalysis" Ed. M. Tsutsui;Plenum Press, New York, 3, 691(1979).

28. N. L. Holy; J. Org. Chem; 44, 239(1979).